Ferrocenyl-Functionalised Terpyridines and Their Transition-Metal Complexes: Syntheses, Structures and Spectroscopic and Electrochemical Properties

Ulrich Siemeling,*[a] Jens Vor der Brüggen,[a] Udo Vorfeld,[a] Beate Neumann,[b] Anja Stammler,[b] Hans-Georg Stammler,[b] Andreas Brockhinke,[b] Regina Plessow,[b] Piero Zanello,[c] Franco Laschi,[c] Fabrizia Fabrizi de Biani,[c] Marco Fontani,[c] Steen Steenken,[d] Marion Stapper,[d] and Gagik Gurzadyan[d]

Abstract: Terpyridine ligands of the type Fc′-X-tpy′ (Fc′ = ferrocenyl or octamethylferrocenyl, X = rigid spacer, tpy′ = 4′-substituted 2,2′:6′,2″-terpyridine) were prepared, crystallographically characterised and used for the synthesis of di- and trinuclear bis(terpyridine) complexes of Ru^{II}, Fe^{II} and Zn^{II}. Donor–sensitiser dyads and triads based on Ru^{II} were thoroughly investigated by (spectro)electrochemistry, UV/Vis, transient absorption and luminescence spectroscopy, and an energy level scheme was derived on the basis of the data collected. Intramolecular quenching of the photoexcited Ru^{II} complexes by the redox-active Fc′ groups can occur reductively and by energy transfer. Both the redox potential of the donor Fc′ and the nature of the spacer X have a decisive influence on excited-state lifetimes and emission properties of the complexes. Some of the compounds show room-temperature luminescence, which is unprecedented for ferrocenyl-functionalised compounds of this kind.

Keywords: electrochemistry · heterometallic complexes · ligand design · luminescence · time-resolved spectroscopy

Introduction

Ruthenium(II) oligopyridine complexes exhibit unique photophysical, photochemical and redox-chemical properties. They are often excellent photosensitisers and have, inter alia, been utilised for this purpose in supramolecular assemblies.[1] Among the oligopyridine ligands 2,2′:6′,2″-terpyridines bearing redox-active groups in the 4′-position are currently attracting much attention, since they can be used for the construction of geometrically well-defined metal complexes which show fascinating properties based on intramolecular electron and energy transfer and may be applied to address fundamental questions concerning such processes.[1g, 2] Owing to their well-behaved redox chemistry, chemical robustness and synthetic versatility, ferrocenyl groups are increasingly utilised as redox-active components in such investigations.[3] Although ferrocene derivatives are commonly known as efficient luminescence quenchers, it has emerged that ferrocenyl groups may be advantageously used as redox centres in multiresponsive, photo- and electrochemically active assemblies.[4]

Here we present results of a study on 2,2′:6′,2″-terpyridine ligands **1a–f** with a ferrocenyl (Fc) or octamethylferrocenyl

tpy'-C≡C-Fc	tpy'-C≡C-Fc$^{\#}$
1a	**1b**
tpy'-*p*-C_6H_4-C≡C-Fc	tpy'-*p*-C_6H_4-C≡C-Fc$^{\#}$
1c	**1d**
tpy'-C≡C-*p*-C_6H_4-C≡C-Fc	tpy'-C≡C-*p*-C_6H_4-C≡C-Fc$^{\#}$
1e	**1f**

[a] Prof. U. Siemeling, Dr. J. Vor der Brüggen, Dr. U. Vorfeld
Department of Physics, University of Kassel
34109 Kassel (Germany)
Fax: (+49) 561-804-4777
E-mail: siemeling@uni-kassel.de

[b] B. Neumann, A. Stammler, Dr. H.-G. Stammler, Dr. A. Brockhinke, R. Plessow
Department of Chemistry, University of Bielefeld
33501 Bielefeld (Germany)

[c] Prof. P. Zanello, Prof. F. Laschi, Dr. F. Fabrizi de Biani, Dr. M. Fontani
Department of Chemistry, University of Siena
53100 Siena (Italy)

[d] Prof. S. Steenken, M. Stapper, Dr. G. Gurzadyan
Max Planck Institute for Radiation Chemistry
45470 Mülheim an der Ruhr (Germany)

 DOI: 10.1002/chem.200204412

group (Fc#) attached to the 4′-position by a rigid spacer comprising acetylene and *para*-phenylene moieties in a series of coordination compounds.[5]

Related work based on 4′-ferrocenyl-2,2′:6′,2″-terpyridine (Fc-tpy′) was recently published by Hutchison et al.[6]

Results and Discussion

Synthesis and structural characterisation of compounds: *Ligands and precursors*: The redox-functionalised ligands used in the present study were synthesised by Sonogashira-type cross-coupling reactions (Scheme 1). Standard protocols[7] could be applied and afforded the coupling products in good yields.

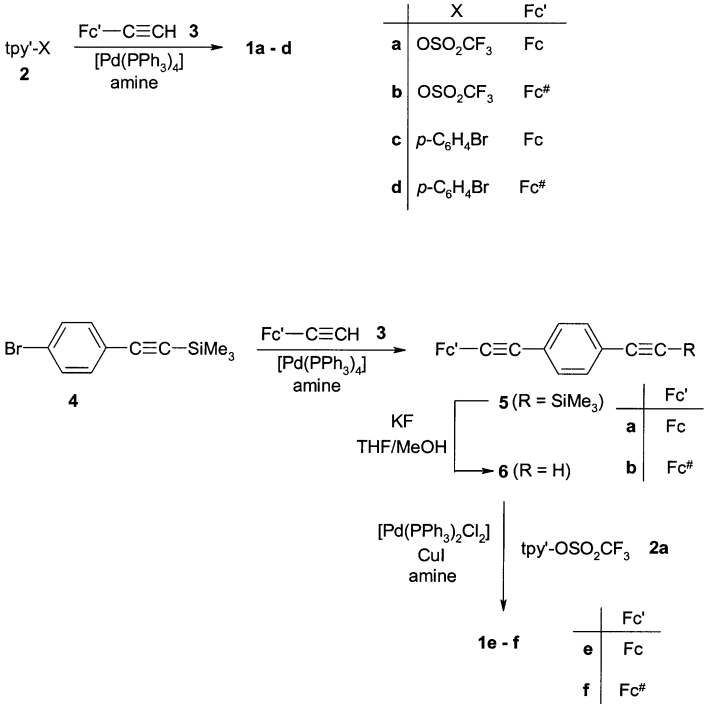

Scheme 1. Synthesis of Fc-C≡C-tpy′ (**1a**), Fc#-C≡C-tpy′ (**1b**), Fc-C≡C-*p*-C_6H_4-tpy′ (**1c**), Fc#-C≡C-*p*-C_6H_4-tpy′ (**1d**), Fc-C≡C-*p*-C_6H_4-C≡C-tpy′ (**1e**) and Fc#-C≡C-*p*-C_6H_4-C≡C-tpy′ (**1f**).

Ligands **1a** and **1b** were obtained from the reaction of 4′-(trifluoromethylsulfonyloxy)-2,2′:6′,2″-terpyridine[8] (**2a**) with ethynylferrocene[9] (**3a**) and ethynyloctamethylferrocene[10] (**3b**), respectively. Ligands **1c** and **1d** were prepared analogously from 4′-(4-bromophenyl)-2,2′:6′,2″-terpyridine (**2b**).[11] Compounds **1e** and **1f** were obtained in a three-step reaction (coupling/deprotection/coupling sequence) utilising 4-bromo-(trimethylsilylethynyl)benzene[12] (**4**) as a building block. The intermediates FcC≡C-*p*-C_6H_4-C≡CSiMe_3 (**5a**) and FcC≡C-*p*-C_6H_4-C≡CH (**6a**) have already been described by Sita et al.[13] **1a**–**f** are air-stable in the solid state. In solution, however, the Fc#-functionalised compounds are prone to oxidation.

Single-crystal X-ray structure determinations were performed for ligands **1a**–**d**, and two representative molecular structures are shown in Figure 1 and Figure 2. Bond lengths

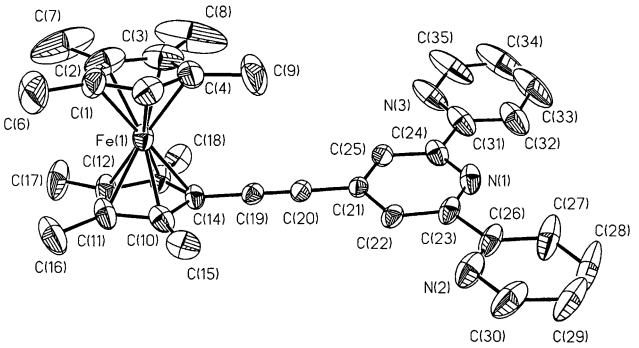

Figure 1. Molecular structure of **1b** in the crystal. Selected bond lengths [pm] and angles [°]: N(1)–C(23) 133.5(5), N(1)–C(24) 134.5(5), N(2)–C(26) 132.8(6), N(2)–C(30) 134.1(6), N(3)–C(31) 134.2(7), N(3)–C(35) 133.9(6), C(14)–C(19) 143.0(5), C(19)–C(20) 119.7(5), C(20)–C(21) 143.5(5), C(23)–C(26) 149.1(6), C(24)–C(31) 147.8(6); C(14)-C(19)-C(20) 179.4(4), C(19)-C(20)-C(21) 177.4(4).

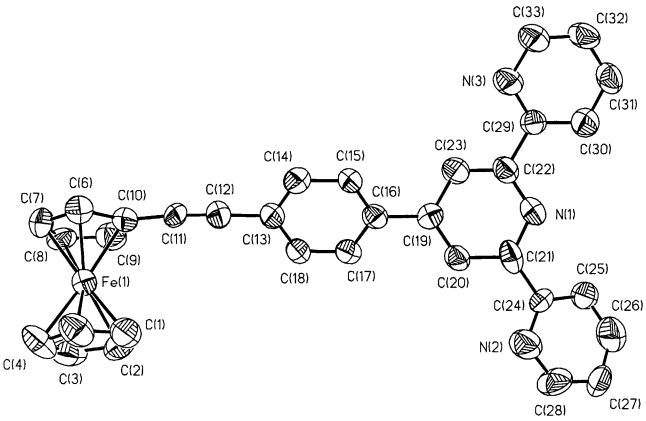

Figure 2. Molecular structure of **1c** in the crystal. Only one of the two individual molecules is shown. Selected bond lengths [pm] and angles [°] for this molecule: N(1)–C(21) 136.8(9), N(1)–C(22) 135.2(8), N(2)–C(24) 135.3(9), N(2)–C(28) 128.2(12), N(3)–C(29) 130.2(9), N(3)–C(33) 135.3(9), C(10)–C(11) 142.7(12), C(11)–C(12) 118.9(12), C(12)–C(13) 146.4(10), C(16)–C(19) 149.6(9), C(21)–C(24) 145.6(15), C(22)–C(29) 149.0(7); C(10)-C(11)-C(12) 175.4(11), C(11)-C(12)-C(13) 175.9(10).

and angles are generally unexceptional. The acetylene groups are almost linear with C≡C distances of about 119 pm. In each case the three C_5N rings exhibit transoid configuations about the interannular C–C bonds, as is commonly observed for such compounds. These rings are almost coplanar (dihedral angles $\leq 10°$), except for **1c**, in which angles between 3.6 and 25.6° are observed, which may be due to crystal packing forces.[14] The cyclopentadienyl rings are arranged in an approximately eclipsed orientation and exhibit very similar average Fe–C bond lengths of about 205 pm, which is nearly identical to the values observed for ferrocene[15] and decamethylferrocene.[16] Owing to steric reasons, the phenylene rings of **1c** (two individual molecules) and **1d** form angles of 36.1/35.3 and 26.9°, respectively, with the central C_5N ring of the terpyridyl unit, and this leads to a reduced degree of π delocalisation (vide infra).

Metal complexes: The metal complexes prepared from the new terpyridines of type **1** are shown in Scheme 2. They were synthesised by established methods.[17]

Homoleptic Ru^{II} complexes

$[(tpy'\text{-}C{\equiv}C\text{-}Fc)_2Ru]^{2+}$ $[(tpy'\text{-}p\text{-}C_6H_4\text{-}C{\equiv}C\text{-}Fc)_2Ru]^{2+}$

$[(\mathbf{1a})_2Ru]^{2+}$ $[(\mathbf{1c})_2Ru]^{2+}$

$[(tpy'\text{-}C{\equiv}C\text{-}p\text{-}C_6H_4\text{-}C{\equiv}C\text{-}Fc)_2Ru]^{2+}$ $(tpy'\text{-}p\text{-}C_6H_4\text{-}C{\equiv}C\text{-}Fc^{\#})_2Ru]^{2+}$

$[(\mathbf{1e})_2Ru]^{2+}$ $[(\mathbf{1d})_2Ru]^{2+}$

Heteroleptic Ru^{II} complexes

$[(tpy'\text{-}C{\equiv}C\text{-}Fc)Ru(tpy)]^{2+}$ $[(tpy'\text{-}p\text{-}C_6H_4\text{-}C{\equiv}C\text{-}Fc)Ru(tpy)]^{2+}$

$[(\mathbf{1a})Ru(tpy)]^{2+}$ $[(\mathbf{1c})Ru(tpy)]^{2+}$

$[(tpy'\text{-}C{\equiv}C\text{-}p\text{-}C_6H_4\text{-}C{\equiv}C\text{-}Fc)Ru(tpy)]^{2+}$ $[(tpy'\text{-}p\text{-}C_6H_4\text{-}C{\equiv}C\text{-}Fc^{\#})Ru(tpy)]^{2+}$

$[(\mathbf{1e})Ru(tpy)]^{2+}$ $[(\mathbf{1d})Ru(tpy)]^{2+}$

$[(tpy'\text{-}p\text{-}C_6H_4\text{-}C{\equiv}C\text{-}Fc)Ru(tpy'\text{-}p\text{-}C_6H_4\text{-}C{\equiv}C\text{-}Fc^{\#})]^{2+}$ $[(tpy'\text{-}C{\equiv}C\text{-}Fc^{\#})Ru(tpy)]^{2+}$

$[(\mathbf{1c})Ru(\mathbf{1d})]^{2+}$ $[(\mathbf{1b})Ru(tpy)]^{2+}$

Ru^{II} complexes with an oxidised ferrocenyl moiety

$[(tpy'\text{-}C{\equiv}C\text{-}Fc)Ru(tpy)]^{3+}$ $[(tpy'\text{-}p\text{-}C_6H_4\text{-}C{\equiv}C\text{-}Fc^{\#})Ru(tpy)]^{3+}$

$[(\mathbf{1a})Ru(tpy)]^{3+}$ $[(\mathbf{1d})Ru(tpy)]^{3+}$

Complexes of metals other than Ru

$[(tpy'\text{-}C{\equiv}C\text{-}Fc)_2Zn]^{2+}$ $[(tpy'\text{-}p\text{-}C_6H_4\text{-}C{\equiv}C\text{-}Fc^{\#})_2Zn]^{2+}$

$[(\mathbf{1a})_2Zn]^{2+}$ $[(\mathbf{1d})_2Zn]^{2+}$

$[(tpy'\text{-}C{\equiv}C\text{-}Fc)_2Fe]^{2+}$

$[(\mathbf{1a})_2Fe]^{2+}$

Scheme 2. Metal complexes prepared and investigated in this work.

Complications in the coordination chemistry towards ruthenium tended to arise with these ligands 1) when they bear an $Fc^{\#}$ group and 2) when the spacer allowed efficient π delocalisation. Reactions of **1b** proved to be particularly temperamental.

Homoleptic ruthenium complexes were obtained from the reaction of two equivalents of the respective terpyridine **1** with $[RuCl_2(dmso)_4]$[18] or hydrated $RuCl_3$. In the latter case a mild reducing agent (triethylamine or *N*-ethylmorpholine) was added. Unfortunately, despite many efforts, $[(\mathbf{1b})_2Ru]^{2+}$ could not be obtained in pure form.

The heteroleptic complexes $[(\mathbf{1c})Ru(tpy)]^{2+}$ and $[(\mathbf{1d})Ru(tpy)]^{2+}$ were synthesised by the reaction of $[(\mathbf{1c})RuCl_2(dmso)]$ and $[(\mathbf{1d})RuCl_2(dmso)]$, respectively, with 2,2′:6′,2″-terpyridine (tpy). $[(\mathbf{1c})Ru(\mathbf{1d})]^{2+}$ was prepared from $[(\mathbf{1c})RuCl_2(dmso)]$ and **1d**, whereas the alternative reaction of $[(\mathbf{1d})RuCl_2(dmso)]$ with **1c** failed. For the synthesis of all other heteroleptic complexes, $[(tpy)RuCl_3]$[19] was allowed to react with one equivalent of the respective terpyridine **1** in the presence of triethylamine or *N*-ethylmorpholine.

Oxidation of the ferrocenyl moiety of $[(\mathbf{1a})Ru(tpy)]^{2+}$ was cleanly achieved with acetylferrocenium tetrafluoroborate to give the tricationic species $[(\mathbf{1a})Ru(tpy)]^{3+}$ in high yield. Similarly, the weaker oxidant ferrocenium hexafluorophosphate was sufficient to oxidise $[(\mathbf{1d})Ru(tpy)]^{2+}$, which contains the more electron-rich $Fc^{\#}$ group. The NMR spectra were often affected by the sensitivity of the $Fc^{\#}$ moiety to oxidation, leading to broad or sometimes even unobservable signals for this unit.

The iron complex $[(\mathbf{1a})_2Fe]^{2+}$ was prepared from iron(II) chloride and two equivalents of **1a**. The zinc complexes $[(\mathbf{1a})_2Zn]^{2+}$ and $[(\mathbf{1d})_2Zn]^{2+}$ were obtained from the reaction of zinc tetrafluoroborate with two equivalents of **1a** and **1d**, respectively. The crystal structure of $[(\mathbf{1a})_2Zn]^{2+}$ was determined by X-ray diffraction (Figure 3). Bond lengths and

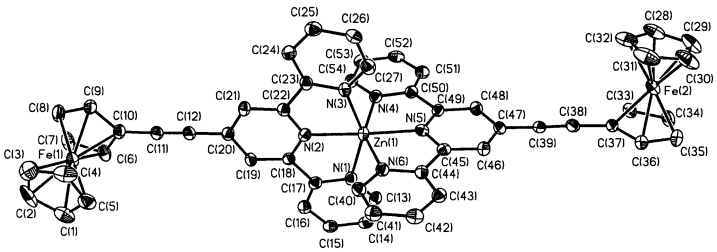

Figure 3. Molecular structure of $[(\mathbf{1a})_2Zn]^{2+}$ in the crystal. Selected bond lengths [pm] and angles [°]: N(1)–C(13) 133.3(4), N(1)–C(17) 135.2(4), N(2)–C(18) 133.9(4), N(2)–C(22) 134.2(4), N(3)–C(23) 135.1(4), N(3)–C(27) 134.5(4), N(4)–C(50) 135.7(4), N(4)–C(54) 134.1(4), N(5)–C(45) 134.3(4), N(5)–C(49) 134.1(4), N(6)–C(40) 133.6(4), N(6)–C(44) 135.3(4), C(10)–C(11) 142.4(4), C(11)–C(12) 121.0(4), C(12)–C(20) 142.0(4), C(17)–C(18) 149.5(4), C(22)–C(23) 148.7(4), C(37)–C(38) 142.0(4), C(38)–C(39) 121.1(4), C(39)–C(47) 141.6(4), C(44)–C(45) 148.6(4), C(49)–C(50) 149.5(4); C(10)-C(11)-C(12) 177.5(3), C(11)-C(12)-C(20) 176.6(3), C(37)-C(38)-C(39) 176.9(3), C(38)-C(39)-C(47) 177.5(3).

angles compare well with those of the few related complexes reported to date.[20] The coordination of the zinc ion is best described as distorted octahedral with two short Zn–N(central) bonds (208.1(2) and 209.0(2) pm) and four long Zn–N(terminal) distances (217.5(2)–219.1(2) pm). The bite angle of **1a** is about 151° (N(1)-Zn(1)-N(3) 150.56(9), N(4)-Zn(1)-N(6) 150.77(9)°). Coordination to zinc has no major effect on the bond parameters of **1a**. Naturally, the C_5N rings of the coordinated ligand exhibit cisoid configurations about the interannular C–C bonds, and their dihedral angles (1.1–3.0°) are even smaller than in uncoordinated **1a** (6.4–7.1°).

Electrochemistry and spectroelectrochemistry: The redox-functionalised terpyridines **1a–f** and their ruthenium complexes were investigated by electrochemical methods. Pertinent data for these ligands are collected in Table 1. Data for ferrocene and some relevant derivatives thereof are included for reference purposes.

Ferrocene is easier to oxidise than **1a**, **1c** and **1e** by 0.16, 0.11 and 0.13 V, respectively. Similarly, oxidation of **1b**, **1d** and **1f** occurs at a potential 0.19, 0.07 and 0.15 V, respectively, more positive than that observed for octamethylferrocene. This is in accord with the electron-withdrawing character of the acetylene group attached to the ferrocene nucleus, which is further enhanced by the terpyridyl unit. This influence of the terpyridyl substituent is weakest in the case of **1c** and **1d**,

Table 1. Formal electrode potentials [V versus SCE], peak-to-peak separation [mV] and colour changes for the one-electron oxidation of the ferrocene derivatives under study (dichloromethane solution, 0.2 M nBu$_4$NPF$_6$ supporting electrolyte).

Compound	$E^{\circ\prime}_{0/+}$	ΔE_p[a]	Original colour (λ_{max} [nm])	Final colour[b] (λ_{max} [nm])
1a	+0.57	85	orange (375)	blue (585)
1b	+0.18	147	orange	green
1c	+0.50	62	yellow (440)	brown (574; 820 flattened)
1d	+0.06	76	orange (480)	olive (640 sh; 840 flattened)
1e	+0.52	61	orange (520)	brown (810 flattened)
1f	+0.14	73	red	olive
FcH	+0.39	80	yellow	green (620)
Fc#H	−0.01	82	pale yellow (430)	green (620 sh; 760 w)
FcC≡CH	+0.52	80	yellow (440)	green (690)
Fc#C≡CH	+0.12	70	yellow	green (640 sh; 780)

[a] Measured at 0.1 V s^{-1}. [b] After exhaustive one-electron oxidation.

in which π delocalisation is attenuated by the *para*-phenylene group directly attached to the terpyridyl moiety (vide supra). In contrast, with C≡C and C≡C-*p*-C$_6$H$_4$-C≡C as spacer, efficient π delocalisation is possible, and hence larger $\Delta E^{0\prime}$ values relative to ferrocene or octamethylferrocene are observed for **1a**, **1b**, **1e** and **1f** than for **1c** and **1d**. As expected, the largest shifts occur with the shortest spacer, namely, the acetylene group (**1a**, **1b**).

Electrochemical data for the metal complexes are collected in Table 2 (dinuclear species) and Table 3 (trinuclear species).

As a representative example, the cyclic voltammogram of [(**1d**)$_2$Ru]$^{2+}$ is shown in Figure 4. The complex undergoes a single, ferrocenyl-centred, electrochemically reversible two-electron oxidation, as well as a well-defined Ru-centred one-electron oxidation, the two cathodic processes being roughly similar in height. In the case of [(**1d**)$_2$Ru]$^{2+}$ the original deep red solution turns deep violet upon exhaustive two-electron oxidation ($E_w = +0.4$ V), a process which proved to be chemically reversible. The chemical reversibility of the two sequential reduction processes prompted us to characterise the mono-reduced species by EPR spectroscopy in order to probe a possible contribution of the metal to the cathodic path. Electrogeneration of the radical monocation was performed at −20 °C to slow down possible decomposition. Figure 5 shows the X-band EPR spectrum of electrogenerated [(**1d**)$_2$Ru]$^{+}$ in frozen glassy solution.

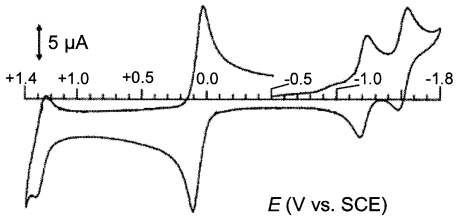

Figure 4. Cyclic voltammetric response recorded at a platinum electrode in a dichloromethane solution of [(**1d**)$_2$Ru]$^{2+}$ (0.6 mM). nBu$_4$NPF$_6$ (0.2 M) supporting electrolyte. Scan rate 0.2 V s^{-1}.

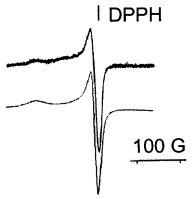

Figure 5. X-band EPR spectrum of electrogenerated [(**1d**)$_2$Ru]$^{+}$ in frozen glassy dichloromethane solution (upper/lower trace: experimental/simulated spectrum). DPPH = 2,2-Diphenyl-1-picrylhydrazyl.

Table 2. Formal electrode potentials [V versus SCE] and peak-to-peak separations [mV] of the redox processes exhibited by the dinuclear complexes under study (dichloromethane solution, 0.2 M nBu$_4$NPF$_6$ supporting electrolyte).

Compound	E(Ru$^{III/II}$)[a,b]	$E^{\circ\prime}$(Fc$^{\prime+/0}$) (ΔE_p[a])	$E^{\circ\prime}$([Ru]$^{2+/+}$) (ΔE_p[a])	$E^{\circ\prime}$([Ru]$^{+/0}$)
[(**1a**)Ru(tpy)]$^{2+}$	+1.33	+0.54 (78)	−1.16 (92)	−1.6
[(**1c**)Ru(tpy)]$^{2+}$	+1.31	+0.55 (67)	−1.18 (65)	−1.58
[(**1d**)Ru(tpy)]$^{2+}$	+1.39	+0.13 (60)	−1.18 (60)	−1.60
[(**1e**)Ru(tpy)]$^{2+}$	+1.36	+0.52 (87)	−1.19 (68)	−1.60

[a] Measured at 0.1 V s^{-1}. [b] Peak-potential value.

Table 3. Formal electrode potentials [V versus SCE] and peak-to-peak separations [mV] of the redox processes exhibited by the trinuclear complexes under study (dichloromethane solution, 0.2 M nBu$_4$NPF$_6$ supporting electrolyte).

Compound	$E^{\circ\prime}$(Ru$^{III/II}$) (ΔE_p[a])	$E^{\circ\prime}$(Fc$^{\prime+/0}$)[b] (ΔE_p[a])	$E^{\circ\prime}$([Ru]$^{2+/+}$) (ΔE_p[a])	$E^{\circ\prime}$([Ru]$^{+/0}$)
[(**1a**)$_2$Ru]$^{2+}$	+1.39 (90)	+0.53 (83)	−1.13 (67)	−1.42
[(**1a**)$_2$Fe]$^{2+}$	+1.1[c] (75)	+0.49 (80)	−1.19[d] (60)	−1.37[e]
[(**1c**)$_2$Ru]$^{2+}$	+1.24 (80)	+0.49 (60)	−1.22 (68)	−1.52
[(**1d**)$_2$Ru]$^{2+}$	+1.27 (85)	+0.06 (98)	−1.21 (80)	−1.52
[(**1e**)$_2$Ru]$^{2+}$	+1.39[a,f]]	+0.52 (62)	−1.22 (65)	−1.52
[(**1f**)$_2$Ru]$^{2+}$	+1.34[a,f]]	+0.08 (70)	−1.10[g]	−1.40[g]
[(**1c**)Ru(**1d**)]$^{2+}$	+1.33 (60)	+0.12 (60), +0.55 (60)	−1.17 (60)	−1.47

[a] Measured at 0.1 V s^{-1}. [b] Two-electron process. [c] $E^{\circ\prime}$(Fe$^{III/II}$). [d] $E^{\circ\prime}$([Fe]$^{2+/+}$). [e] $E^{\circ\prime}$([Fe]$^{+/0}$). [f] Peak-potential value for processes affected by adsorption at the electrode surface. [g] Poorly resolved.

Anisotropic lineshape analysis was carried out by assuming an $S = 1/2$ electron-spin Hamiltonian in which the Zeeman interaction is the main magnetic term. The typical axial resolution exhibits g values that account well for the presence of a paramagnetic species with significant metallic character. Best-fit computer simulation[21] afforded $g_\parallel > g_\perp > g_{electron} = 2.0023$, with $g_\parallel = 2.098(4)$, $g_\perp = 2.008(4)$, $\Delta H_\parallel = 41(4)$ G, $\Delta H_\perp = 14(4)$ G. As a consequence of the significant anisotropic line broadening the lineshape in the glassy state (first- and second-derivative modes) does not give evidence for any hyperfine (^{99}Ru, $I = 5/2$, natural abundance 12.7 %; ^{101}Ru, $I = 5/2$, natural abundance 17.0 %) or superhyperfine (^{14}N, $I = 1$, natural abundance 99.6 %) coupling.

On raising the temperature, the intensity of the signal decreases and the overall linewidth increases until, at the glassy–fluid phase transition ($T = 178$ K), the solution becomes EPR-mute. This spectral behaviour must be attributed to effective intra/intermolecular dynamics experienced by the paramagnetic ruthenium complex under fast-motion conditions (which in turn produce active electron-spin relaxation processes) rather than to chemical instability of the monocation. In fact, rapidly refreezing the fluid solution quantitatively restored the signal of the frozen glassy solution.

The other complexes show essentially similar redox-chemical behaviour (Table 2 and Table 3), and on the basis of all data presented, a number of general trends can be made out. Firstly, the redox processes of the central bis(terpyridine)-ruthenium unit are only slightly influenced by the substituents attached to the 4′-position of the terpyridine ligands. When comparing the ruthenium complexes of **1** with pristine $[Ru(tpy)_2]^{2+}$, no overall tendency is obvious for the $Ru^{III/II}$ couples ($E^{0\prime}$ between 1.24 and 1.39 V versus 1.27 V for $[Ru(tpy)_2]^{2+}$[1f]), whereas their first reduction invariably occurs at less negative potential, indicative of a slightly lower LUMO energy ($E^{0\prime}$ between -1.13 and -1.22 V versus -1.27 V for $[Ru(tpy)_2]^{2+}$[1f]).

Secondly, when comparing individual pairs of the type $[(\mathbf{1})Ru(tpy)]^{2+}/[(\mathbf{1})_2Ru]^{2+}$, one would expect the ruthenium-centred oxidation to be easier for the heteroleptic complexes than for the homoleptic ones, since in the latter case two, instead of one, oxidised ferrocenyl groups are present. The expected behaviour is indeed observed for the pair $[(\mathbf{1a})Ru(tpy)]^{2+}/[(\mathbf{1a})_2Ru]^{2+}$, whereas for complexes of **1c** and **1d** just the opposite is true. A similar unexpected behaviour was observed for the related species $[(Fc\text{-}tpy')Ru(tpy)]^{2+}$ and $[(Fc\text{-}tpy')_2Ru]^{2+}$,[6] whereas analogous complexes of the ligand Fc-*p*-C_6H_4-tpy′ showed the expected behaviour.[1g]

Thirdly, the redox potential of the ferrocenyl moieties present in the terpyridines **1** is almost unaffected by complexation, and hence the $|\Delta E^{0\prime}|$ values are rather small (0.01 to 0.07 V). For the homoleptic complexes $[(\mathbf{1})_2Ru]^{2+}$ a single redox wave is observed for the two identical ferrocenyl groups present, which demonstrates that there is no electronic communication between them. In this context it is useful to inspect the cyclic voltammetric behaviour of the heteroleptic trinuclear complex $[(\mathbf{1c})Ru(\mathbf{1d})]^{2+}$ (Figure 6), the two different ferrocenyl units of which are oxidised at different

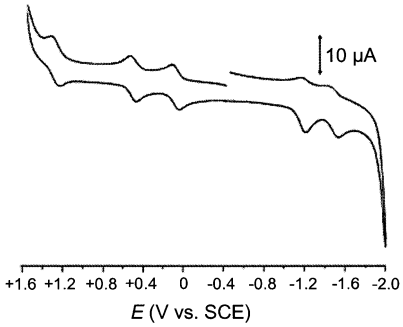

Figure 6. Cyclic voltammogram recorded at a platinum electrode in a dichloromethane solution of $[(\mathbf{1c})Ru(\mathbf{1d})]^{2+}$ (1.2 mM). nBu_4NPF_6 (0.2 M supporting electrolyte. Scan rate 0.2 V s^{-1}.

potentials, each of which is essentially identical with that of the respective dinuclear species (Table 2). This result points out how difficult it is to comment on the intramolecular communication between two inequivalent redox centres. The electrogenerable mixed-valence trication $[(\mathbf{1c})Ru(\mathbf{1d})]^{3+}$ (which substantially maintains the red colour of the parent dication, passing from carmine to ruby red) most likely belongs to the charge-localised Class I according to Robin and Day, in spite of two separate ferrocenyl-centred oxidation processes.

In conclusion, these findings indicate that, irrespective of the spacers used, the redox centres of the ruthenium complexes investigated are essentially independent of one another in the ground state. This is a prerequisite for obtaining meaningful results from a comparative study. Furthermore, when comparing the $Fc^{\#}$-functionalised species with their respective Fc analogues, it is evident that octamethylation generally leads to a cathodic shift of the $E^{0\prime}$ values of about 0.4 V for the ferrocenyl-centred redox processes. This is the value expected for the influence of eight methyl groups (ca. 8×0.05 V) and shows that in the present system oligomethylferrocenyl groups behave as reliable donors with predictable and precisely adjustable redox potentials.

UV/Vis spectroscopy: UV/Vis spectroscopic data are collected in Table 4 for the ligands **1** and metal complexes which could be obtained in analytically pure form. Data for parent compounds are given for reference purposes.

Table 4. UV/Vis spectroscopic data (acetonitrile, 298 K).

Compound	Principal absorption bands ($\lambda_{max} > 250$ nm)[a] λ_{max} [nm] ($\varepsilon \times 10^{-3}$ [M^{-1}cm^{-1}])	Lowest energy band λ_{max} [nm] ($\varepsilon \times 10^{-3}$ [M^{-1}cm^{-1}])
FcH		440 (0.095)
$Fc^{\#}H$		428 (0.123)
$[Ru(tpy)_2]^{2+}$	270 (40.9), 307 (66.7)	475 (15.3)
1a	253 (30.4), 280 (34.0), 321 (21.3), 375 (sh)	450 (1.6)
$[(\mathbf{1a})Ru(tpy)]^{2+}$	273 (63.6), 309 (81.4)	489 (28.7)
$[(\mathbf{1a})Ru(tpy)]^{3+}$	272 (59.8), 308 (73.4)	481 (26.0)
$[(\mathbf{1a})_2Ru]^{2+}$	277 (63.1), 314 (69.8)	505 (28.0)
$[(\mathbf{1a})_2Fe]^{2+}$	283 (82.1), 325 (82.4), 335 (82.5)	585 (52.2)
$[(\mathbf{1a})_2Zn]^{2+}$	282 (73.5), 332 (74.6)	508 (12.9)
1b	281 (50.4), 331 (24.5), 390 (sh)	495 (2.9)
1c	255 (30.9), 290 (48.2), 322 (36.7), 360 (sh)	450 (2.0)
$[(\mathbf{1c})Ru(tpy)]^{2+}$	272 (50.0), 308 (80.5)	487 (28.1)
$[(\mathbf{1c})_2Ru]^{2+}$	275 (58.6), 313 (84.7)	497 (42.4)
1d	253 (39.2), 288 (44.9), 325 (34.8), 400 (sh)	482 (3.2)
$[(\mathbf{1d})Ru(tpy)]^{2+}$	272 (48.9), 309 (69.7)	485 (28.1)
$[(\mathbf{1d})Ru(tpy)]^{3+}$	281 (51.3), 308 (73.9)	487 (28.4)
$[(\mathbf{1d})_2Ru]^{2+}$	284 (72.7), 311 (85.5)	495 (40.4)
$[(\mathbf{1d})_2Zn]^{2+}$	284 (77.2), 341 (58.2), 368 (49.4)	533 (7.5)
1e	255 (19.7), 291 (27.4), 321 (21.3), 375 (sh)	450 (2.0)
$[(\mathbf{1e})Ru(tpy)]^{2+}$	272 (47.9), 308 (64.6)	494 (26.8)
$[(\mathbf{1e})_2Ru]^{2+}$	279 (71.7), 333 (93.1)	503 (49.0)
1f	253 (23.5), 287 (29.5), 336 (28.3), 410 (sh)	490 (3.0)

[a] Several additional weaker bands and unresolved shoulders can be observed (cf. Figure 15).

With the exception of the lowest energy band, the UV/Vis absorptions of the complexes of **1** may be viewed, to a first approximation, as the sum of the absorptions of the individual components, namely, the central bis(terpyridine)metal chromophore and the uncoordinated ligand **1**.

The weak absorption band of ferrocene at 440 nm was previously assigned to the $^1A_{1g} \rightarrow {}^1E_{2g}$ ligand-field transition in

D_{5d} symmetry.[22] The corresponding absorption of the more electron-rich octamethylferrocene is observed at 428 nm. The longest wavelength band of **1a**, **1c** and **1e** is red-shifted relative to ferrocene by 10 nm. The corresponding red shift observed for **1b**, **1d** and **1f** relative to octamethylferrocene is about 60 nm. This is in accord with the electron-withdrawing effect of the acetylene group attached to the ferrocene nucleus. A hyperchromic shift of this band is observed in each case.

The longest wavelength absorption of $[Ru(tpy)_2]^{2+}$ at 475 nm is an intense metal-to-ligand charge-transfer (MLCT) band, which has been the object of some scrutiny. Essentially, this band corresponds to the ruthenium-based transition $^1[(d(\pi)^6)] \rightarrow {}^1[(d(\pi)^5)(\pi^*_{tpy})^1]$ and its vibronic components.[1f] In the redox-functionalised complexes which contain ligands of type **1**, this band experiences a bathochromic as well as a hyperchromic shift. This red shift is about 10 nm larger for species of the type $[(\mathbf{1})_2Ru]^{2+}$, which contain two ferrocenyl groups, than for the corresponding heteroleptic $[(\mathbf{1})Ru(tpy)]^{2+}$. In all cases but one, homoleptic complexes show a larger hyperchromic shift of this band (by a factor of 1.4–1.8) than their heteroleptic analogues. The exception is the pair $[(\mathbf{1a})_2Ru]^{2+}/[(\mathbf{1a})Ru(tpy)]^{2+}$, which have almost identical extinction coefficients. For comparison, identical ε values have also been reported for the pair $[(Fc\text{-}tpy')_2Ru]^{2+}/[(Fc\text{-}tpy')Ru(tpy)]^{2+}$,[6] whereas in the case of $[(Fc\text{-}p\text{-}C_6H_4\text{-}tpy')_2Ru]^{2+}/[(Fc\text{-}p\text{-}C_6H_4\text{-}tpy')Ru(tpy)]^{2+}$ the ratio of extinction coefficients is 1.2 for this band.[1g]

We pause to remind ourselves that the electrochemical behaviour of the pair $[(Fc\text{-}tpy')_2Ru]^{2+}/[(Fc\text{-}tpy')Ru(tpy)]^{2+}$ was counter-intuitive, whereas that of $[(\mathbf{1a})_2Ru]^{2+}/[(\mathbf{1a})Ru(tpy)]^{2+}$ was just as expected (larger value of $E^{0\prime}(Ru^{III/II})$ for the homoleptic complex, vide supra). In summary, $[(\mathbf{1a})_2Ru]^{2+}/[(\mathbf{1a})Ru(tpy)]^{2+}$ and $[(Fc\text{-}tpy')_2Ru]^{2+}/[(Fc\text{-}tpy')Ru(tpy)]^{2+}$ show quite different electrochemistry, but very similar UV/Vis spectroscopic properties. This discrepancy may be a consequence of the fact that cyclic voltammetry probes the ground state of the redox-active species involved, whereas UV/Vis spectroscopy probes excited states.

Closer inspection reveals that the UV/Vis spectra of all complexes of **1** exhibit a shoulder on the low-energy side of the longest wavelength absorption band. A similar observation was made for $[(Fc\text{-}tpy')_2Ru]^{2+}$ and $[(Fc\text{-}tpy')Ru(tpy)]^{2+}$, for which, on the basis of resonance Raman data, this shoulder was assigned to the ferrocenyl-based MLCT transition $^1[(d(\pi)^6_{Fc})] \rightarrow {}^1[(d(\pi)^5_{Fc})(\pi^{*Ru}_{tpy})^1]$.[6] We investigated the origin of this shoulder in some detail for the heteroleptic complexes $[(\mathbf{1a})Ru(tpy)]^{2+}$ and $[(\mathbf{1d})Ru(tpy)]^{2+}$. The shoulder shows solvatochromism and is more evident in solvents of lower polarity than acetonitrile (see Figure 15 for EtOH/MeOH 4/1). Oxidation of the (octamethyl)ferrocenyl moiety leads to a remarkable decrease in the intensity of the shoulder, which therefore is in agreement with a ferrocenyl-based transition. A difference spectrum is in accord with an assignment of the shoulder as a band centred at 525 nm for $[(\mathbf{1a})Ru(tpy)]^{2+}$ (Figure 7) and at 532 nm for $[(\mathbf{1d})Ru(tpy)]^{2+}$ (Figure 8). We note that this band cannot be due to Fe^{II} impurities, since the absorption maxima of $[Fe(tpy)_2]^{2+}$, $[(\mathbf{1a})_2Fe]^{2+}$ and $[(Fc\text{-}tpy')_2Fe]^{2+}$[6] are at much longer wavelengths (562, 585 and 587 nm, respectively). The fact that the longest wavelength absorptions of the zinc complexes $[(\mathbf{1a})_2Zn]^{2+}$ and $[(\mathbf{1d})_2Zn]^{2+}$ are observed at 508 and 533 nm, respectively, corroborates that this band corresponds to a ferrocenyl-based MLCT transition. Unsurprisingly, in comparison to the Fc unit the more electron-rich Fc# moiety effects an absorption at lower energy, the difference between the two bands being 0.12 eV in this case.

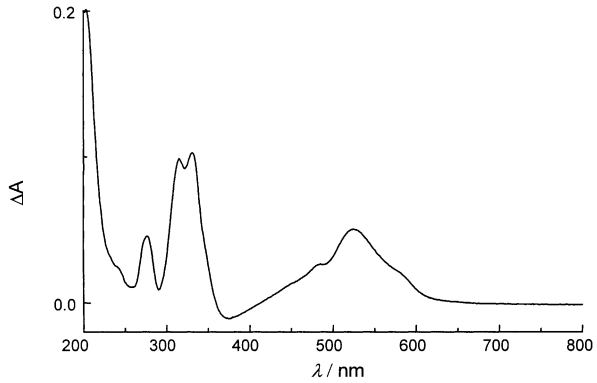

Figure 7. Difference spectrum: $\Delta A = A([(\mathbf{1a})Ru(tpy)]^{2+}) - A([(\mathbf{1a})Ru(tpy)]^{3+})$.

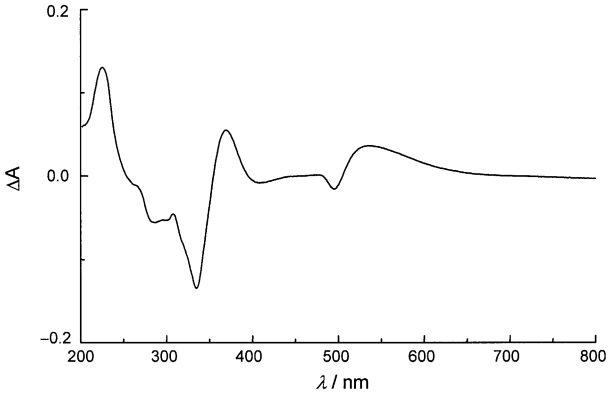

Figure 8. Difference spectrum: $\Delta A = A([(\mathbf{1d})Ru(tpy)]^{2+}) - A([(\mathbf{1d})Ru(tpy)]^{3+})$.

Transient absorption spectroscopy: Photophysical processes occurring after photoexcitation involve transient species, which can be investigated by (ultra)fast spectroscopic techniques. Bis(terpyridine)ruthenium(II) complexes generally exhibit rather short excited-state lifetimes at room temperature. According to Hutchison et al.[6] the lifetimes of photoexcited $[(Fc\text{-}tpy')_2Ru]^{2+}$ and $[(Fc\text{-}tpy')Ru(tpy)]^{2+}$ are shorter than the resolution limit of their experimental setup (20 ns). The photophysical properties of pristine $[Ru(tpy)_2]^{2+}$ in aqueous solution have already been described by Sutin et al.,[23] who found the mean lifetime of the ^{3}MLCT state to be 250 ps. Due to solubility reasons, we used water/acetonitrile mixtures in the present study (2/3 for picosecond experiments, 4/1 for nanosecond experiments). In this solvent system photoexcited $[Ru(tpy)_2]^{2+}$ has a mean lifetime τ of only 120 ps (Figure 9, Table 5).

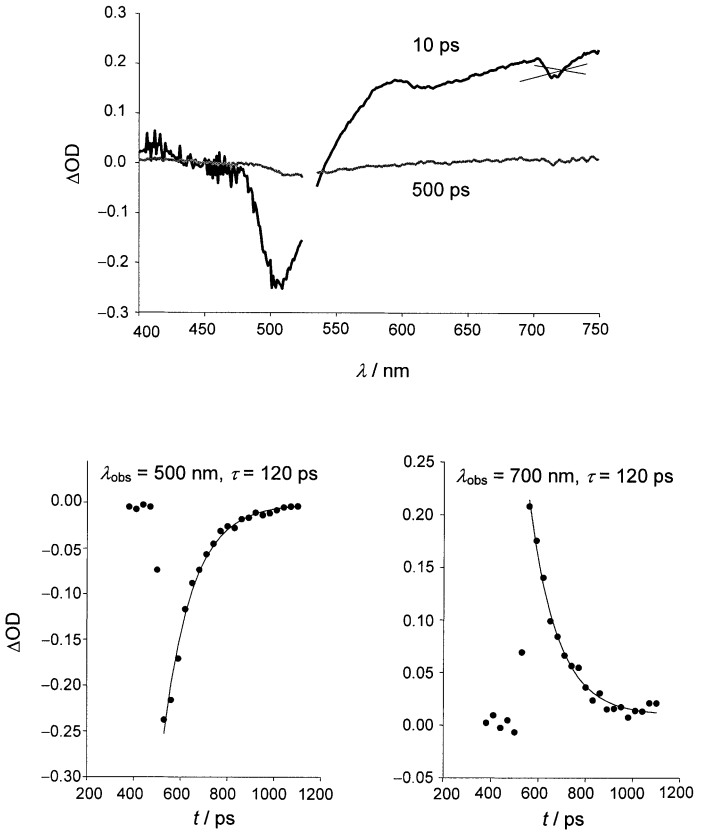

Figure 9. Absorption spectra (top) of transients from the photolysis of $[(tpy)_2Ru]^{2+}$ in water/acetonitrile (2/3), 10 (black) and 500 ps (grey) after the laser flash. The kinetic traces (bottom) show that all bands belong to only one species.

Table 5. Excited-state mean lifetimes measured by laser flash photolysis ($\lambda_{obs} = 650$ nm).

Compound	τ [ns]	Compound	τ [ns]
$[(tpy)_2Ru]^{2+}$	0.12[a]	$[(\mathbf{1c})_2Ru]^{2+}$	<20[c]
$[(\mathbf{1a})_2Ru]^{2+}$	260[b]	$[(\mathbf{1c})Ru(tpy)]^{2+}$	<20[c]
$[(\mathbf{1a})Ru(tpy)]^{2+}$	260[b, c]	$[(\mathbf{1e})_2Ru]^{2+}$	110[b]
$[(\mathbf{1a})Ru(tpy)]^{3+}$	250[b]	$[(\mathbf{1e})Ru(tpy)]^{2+}$	120[b]

[a] Water/acetonitrile (2/3), RT, $\lambda_{exc} = 480$ nm, laser pulse width 30 ps. [b] Water/acetonitrile (4/1), RT, $\lambda_{exc} = 480$ nm, laser pulse width 20 ns. [c] Water/acetonitrile (4/1), RT, $\lambda_{exc} = 308$ nm, laser pulse width 20 ns.

The mean lifetime of the ruthenium-based ^{3}MLCT state of $[(\mathbf{1a})Ru(tpy)]^{2+}$ was determined to be 260 ns by time-resolved transient absorption spectroscopy at $\lambda_{obs} = 670$ nm with different excitation wavelengths ($\lambda_{exc} = 308$ and 480 nm) (Figure 10). Bleaching of the ground state is observed at about 480 nm, whereas the increase in optical density (OD) around 400 and 680 nm is typical of reduced oligopyridine ligands.[23] Monitoring ΔOD at wavelengths shorter than about 600 nm reveals that the decay of this state is superimposed by a much faster process (vide infra; Figure 11).

The oxidised species $[(\mathbf{1a})Ru(tpy)]^{3+}$ gives essentially the same result for the long-lived state ($\tau = 250$ ns). This indicates that the long-lived state is independent of the ferrocenyl unit. The long-lived ruthenium-based ^{3}MLCT state of both $[(\mathbf{1a})Ru(tpy)]^{2+}$ and $[(\mathbf{1a})Ru(tpy)]^{3+}$ is quenched by oxygen,

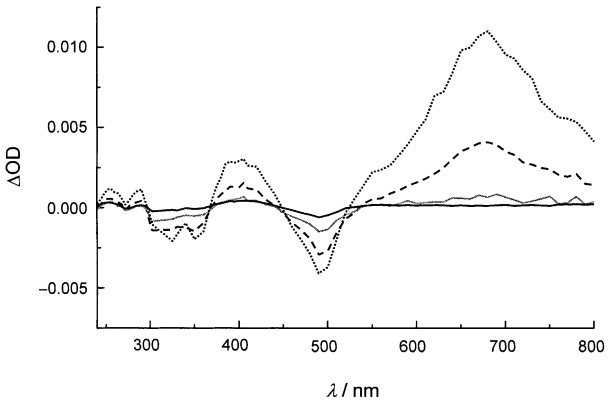

Figure 10. Absorption spectra of transients from the photolysis of $[(\mathbf{1a})Ru(tpy)]^{2+}$ in water/acetonitrile (4/1), RT, recorded 80 ns (dotted), 300 ns (dashed), 700 ns (grey) and 15 μs (solid) after the laser flash.

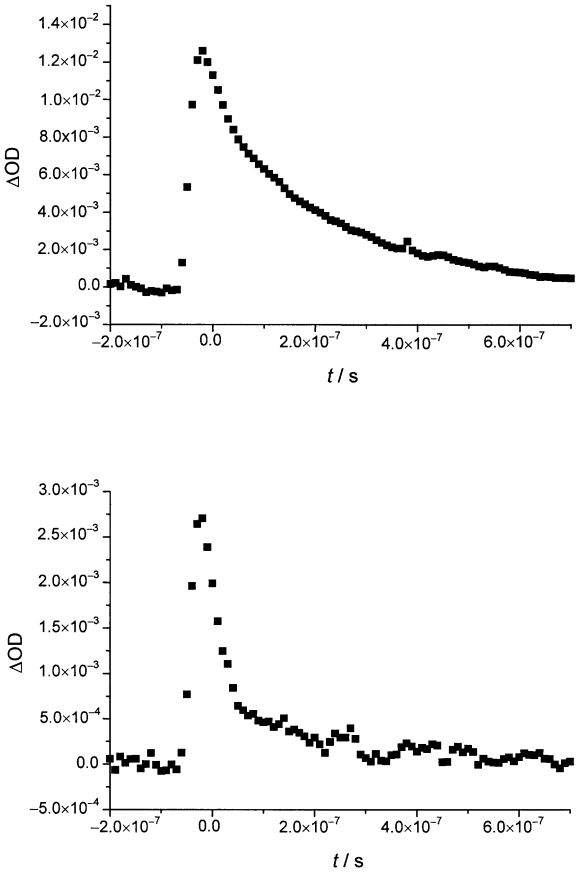

Figure 11. Kinetic traces recorded at 540 (bottom) and 670 nm (top) in transient absorption spectroscopy with $[(\mathbf{1a})Ru(tpy)]^{2+}$.

as is typical of a triplet species. Similar to the results obtained in the nanosecond time regime, experiments with $[(\mathbf{1a})Ru(tpy)]^{2+}$ in water/acetonitrile (2/3) in the femtosecond time regime ($\lambda_{exc} = 400$ nm, pulse width 130 fs) show immediate bleaching of the ground state and formation of a broad absorption peaking at about 670 nm, which remains almost constant during the time window of the experiment (0–900 ps).[24]

Regardless of the Fc oxidation state, introduction of the FcC≡C substituent leads to a lengthening of the ^{3}MLCT state

lifetime by three orders of magnitude. A similar effect is observed for the FcC≡C-*p*-C_6H_4C≡C substituent. This effect is not totally unexpected, since Ziessel, Harriman et al.[25] have shown for bis(terpyridine)ruthenium(II) complexes that introduction of acetylenic substituents in the 4′-position of tpy can lead to a dramatic increase in excited state lifetimes, which ultimately is due to strong electronic coupling between the π systems of the terpyridine and the acetylene. This coupling is interrupted by the *para*-phenylene group present in **1c**, which, owing to steric reasons, is not coplanar with the terpyridine ring it is attached to (vide supra). Essentially the same holds true for Fc-tpy′, in the single crystal of which the cyclopentadienyl ring forms an angle of 19.2° with the central C_5N ring.[26] Similar to $[(Fc\text{-}tpy')_2Ru]^{2+}$ and $[(Fc\text{-}tpy')Ru(tpy)]^{2+}$,[6] the mean lifetimes of photoexcited $[(\mathbf{1c})Ru(tpy)]^{2+}$ and $[(\mathbf{1c})_2Ru]^{2+}$ lie well below 20 ns (Table 5).

Experiments in the picosecond time regime with $\lambda_{exc} = 532$ nm revealed that a short-lived transient with a mean lifetime of about 2 ns is formed for all Fc-functionalised complexes (Table 6). In each case, this transient gives rise to an increase in absorbance with a maximum ΔOD around 540–550 nm (Figure 12), which is absent in the case of the oxidised species $[(\mathbf{1a})Ru(tpy)]^{3+}$ (Figure 13).

Table 6. Excited state mean lifetimes measured by laser flash photolysis (water/acetonitrile (2/3), RT, $\lambda_{exc} = 532$ nm, laser pulse width 30 ps, $\lambda_{obs} = 540$ nm).

Compound	τ [ns]	Compound	τ [ns]
$[(\mathbf{1a})_2Ru]^{2+}$	2	$[(\mathbf{1c})Ru(tpy)]^{2+}$	1.6
$[(\mathbf{1a})Ru(tpy)]^{2+}$	4	$[(\mathbf{1e})Ru(tpy)]^{2+}$	1.6
$[(\mathbf{1a})Ru(tpy)]^{3+}$	– [a]	$[(\mathbf{1e})Ru(tpy)]^{2+}$	1.7
$[(\mathbf{1c})_2Ru]^{2+}$	1.8		

[a] Not observed.

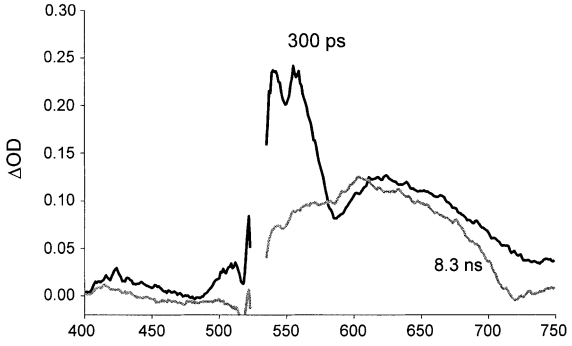

Figure 12. Absorption spectra of transients from the photolysis of $[(\mathbf{1a})Ru(tpy')]^{2+}$ in water/acetonitrile (2/3), RT, 300 ps (black) and 8.3 ns (grey) after the laser flash.

No such transient was observed in the experiments performed with $[(\mathbf{1a})Ru(tpy)]^{2+}$ in the femto/picosecond time regime. In this case, the excitation wavelength ($\lambda_{exc} = 400$ nm) was well below the low-energy shoulder of the longest wavelength absorption of this compound. These results indicate that the absorption around 540–550 nm is most likely associated with the ferrocenyl moiety and may be

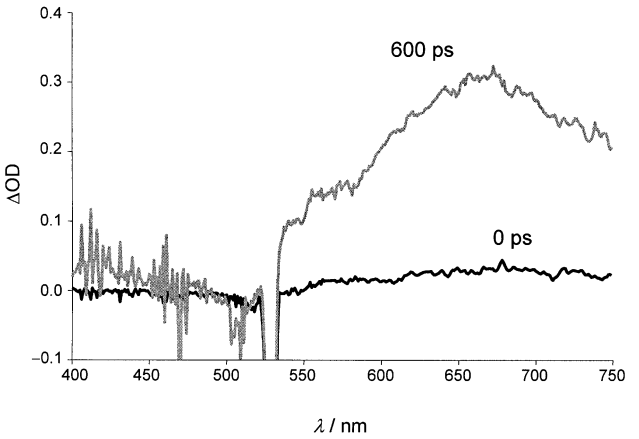

Figure 13. Absorption spectra of transients from the photolysis of $[(\mathbf{1a})Ru(tpy)]^{3+}$ in water/acetonitrile (2/3), 0 (black) and 600 ps (grey) after the laser flash.

attributed to the charge-separated $^3[(d(\pi)^5_{Fc})(\pi^{*Ru}_{tpy})^1]$ state produced by the ferrocenyl-based MLCT transition $^1[(d(\pi)^6_{Fc})] \rightarrow {}^1[(d(\pi)^5_{Fc})(\pi^{*Ru}_{tpy})^1]$.

We performed experiments with $[(\mathbf{1a})Ru(tpy)]^{2+}$ in the presence of triethylamine, which may act as a reductive quencher. High concentrations of NEt_3 (>0.1 M) quench the transient species responsible for the absorbance increase at about 550 nm. This behaviour is compatible with the assignment of this short-lived species as the $^3[(d(\pi)^5_{Fc})(\pi^{*Ru}_{tpy})^1]$ excited state, which is reductively quenched by NEt_3. The bimolecular quenching reaction must be considerably faster than the decay of the transient species. A meaningful Stern–Volmer analysis was not possible due to the limited kinetic data available.

Photoexcitation ($\lambda_{exc} = 532$ nm) of the Fc#-substituted complexes $[(\mathbf{1d})Ru(tpy)]^{2+}$ and $[(\mathbf{1d})_2Ru]^{2+}$ leads to transient species with rather short mean lifetimes. The maximum ΔOD is observed at 630 nm for $[(\mathbf{1d})Ru(tpy)]^{2+}$, which is in the region typical of reduced terpyridine ligands. Time-resolved measurements at this wavelength gave a mean lifetime of 90 ps. The corresponding τ value for $[(\mathbf{1d})_2Ru]^{2+}$ is 160 ps, and a second, even shorter lived transient ($\tau \approx 10$ ps, max ΔOD 540 nm) can be observed for this homoleptic complex. These short τ values are in accord with, but do not prove, the assumption that in the present system the higher thermodynamic driving force for reductive quenching operative for Fc# versus Fc derivatives coincides with faster electron transfer rates.

Luminescence spectroscopy: Terpyridine complexes of Ru^{II} usually show much weaker room-temperature luminescence than their bipyridine relatives, whereas at low temperatures the opposite is often the case (Table 7).[1f] In comparison to $[Ru(tpy)_2]^{2+}$, ferrocenyl-substituted analogues show almost negligible luminescence (Table 7).

The Fc moiety acts as an efficient quencher for the ^{3}MLCT state in such species, and to date no example of room-temperature luminescence is known for this class of compounds. Ferrocene can quench photoexcited states by two mechanisms, that is, reductively and by energy transfer.[1g, 3] The redox potential of ferrocene can be changed systemati-

Table 7. Emission maxima, quantum yields and lifetimes for a range of Ru^{II} oligopyridine complexes (EtOH/MeOH 4/1, 77 K).

	λ_{max} [nm][a]	Φ	τ [μs]
$[Ru(bpy)_3]^{2+}$[27]	584, 630	0.38	5.2
$[Ru(tpy)_2]^{2+}$[27, 28]	599, 648	0.48	11.0
$[(Fc\text{-}tpy')Ru(tpy)]^{2+}$[6]	601, 649	ca. 0.003	< 0.025
$[(Fc\text{-}typ')_2Ru]^{2+}$[6][b]	599, 648	< 0.003	< 0.025
$[(Fc\text{-}p\text{-}C_6H_4\text{-}tpy')_2Ru]^{2+}$[1g]	–[c]	–[c]	–[c]

[a] Wavelength of the first vibronic components. [b] The authors cannot exclude that the weak emission is due to traces of $[Ru(tpy)_2]^{2+}$. [c] Value could not be determined.

cally by attaching methyl groups to the cyclopentadienyl rings,[29] whereas the triplet energy remains essentially unaffected.[30] Unlike other metallocenes, ferrocenes are not at all phosphorescent (and very likely also not fluorescent).[3]

We studied the emission of a range of ferrocenyl- and octamethylferrocenyl-functionalised complexes at 77 K (Figure 14) and at room temperature by laser-induced luminescence spectroscopy. $Fc^{\#}$-substituted species were nonluminescent at room temperature.

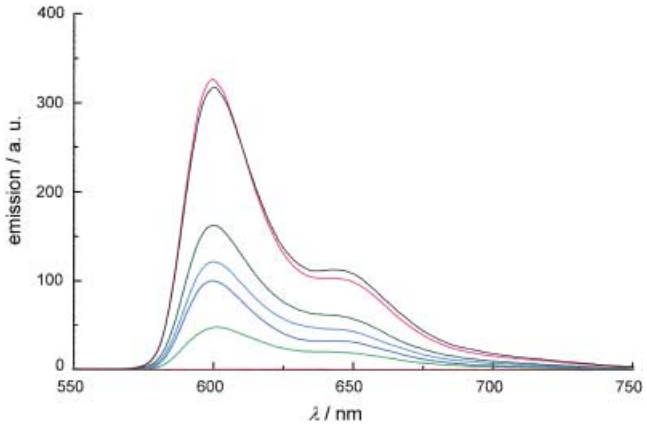

Figure 14. Emission spectra at 77 K, EtOH/MeOH (4/1), $\lambda_{exc} = 480$ nm. Emission intensities [arbitrary units] at the emission maximum: $[(\mathbf{1a})_2Ru]^{2+}$ (red) 0, $[(\mathbf{1d})Ru(tpy]^{2+}$ (green) 48, $[(\mathbf{1a})Ru(tpy)]^{2+}$ (blue) 101, $[(\mathbf{1c})Ru(tpy)]^{2+}$ (cyan) 124, $[(\mathbf{1e})Ru(tpy)]^{2+}$ (olive) 168, $[(\mathbf{1a})Ru(tpy)]^{3+}$ (magenta) 322, $[Ru(tpy)_2]^{2+}$ (black, emission intensity × 0.1) 3283.

The homoleptic $[(\mathbf{1a})_2Ru]^{2+}$, which contains two ferrocenyl units, shows no luminescence at 77 K in frozen glassy solution, whereas the heteroleptic complexes, which contain one Fc′ moiety, are weakly emissive in comparison to $[Ru(tpy)_2]^{2+}$. This finding is in line with the general observation that ferrocenyl units act as efficient quenchers.[3] The heteroleptic compound showing the lowest emission intensity at 77 K is the $Fc^{\#}$-functionalised $[(\mathbf{1d})Ru(tpy]^{2+}$. This is in accord with, but does not prove, the expectation that an increase in the thermodynamic driving force for reductive quenching will favour this mechanism and is also in line with the extremely short τ values observed for the $Fc^{\#}$ derivatives by transient absorption spectroscopy (vide supra). The series of Fc-functionalised dicationic complexes shows a significant effect of the spacer unit, with the longest spacer (C≡C-*p*-C_6H_4-C≡C) leading to the highest, and the shortest spacer (C≡C) to the lowest, emission intensity. Oxidation of the ferrocenyl moiety in $[(\mathbf{1a})Ru(tpy)]^{2+}$ leads to a marked increase in emission intensity. In this case reductive quenching is no longer possible.

For the room-temperature luminescence studies, different solvents were used: acetonitrile; water/acetonitrile (4/1), which was also used for transient absorption spectroscopy in the nanosecond time regime; and EtOH/MeOH (4/1), which was also used for luminescence studies at 77 K. Emission in pure acetonitrile was extremely weak in all cases. Solubility of the compounds in water was too low to allow measurements. Pertinent data are collected in Table 8. Emission maxima were determined from the excitation-emission spectra described below. Quantum yields were determined by using the approach proposed by Demas and Crosby.[31] $[Ru(bpy)_3]^{2+}$ was used as reference standard.

Table 8. Room-temperature luminescence data (deaerated solutions).

	Absorption λ_{max} [nm]	Emission λ_{max} [nm](λ_{exc} [nm])	$\Phi \times 10^5$
$[(\mathbf{1a})Ru(tpy)]^{2+}$[a]	480	699	40 (489)[b]
$[(\mathbf{1a})Ru(tpy)]^{2+}$[c]	484	698	1.5 (490)
$[(\mathbf{1a})Ru(tpy)]^{3+}$[a]	479	698	52 (490)[b]
$[(\mathbf{1a})Ru(tpy)]^{3+}$[c]	479	711	3.5 (490)
$[(\mathbf{1a})Ru(tpy)]^{3+}$[d]	479	706	0.3 (490)
$[(\mathbf{1a})_2Ru]^{2+}$[a]	498	697	84 (498)[b]
$[(\mathbf{1a})_2Ru]^{2+}$[c]	502	693	0.2 (490)
$[(\mathbf{1c})Ru(tpy)]^{2+}$[a]	479	672	6.5 (490)
$[(\mathbf{1c})Ru(tpy)]^{2+}$[c]	487	–[e]	–[e]
$[(\mathbf{1e})Ru(tpy)]^{2+}$[a]	489	688	64 (491)[b]
$[(\mathbf{1e})Ru(tpy)]^{2+}$[c]	493	682	1.0 (490)
$[(\mathbf{1e})Ru(tpy)]^{2+}$[d]	494	688	0.2 (490)

[a] Water/acetonitrile (4/1). [b] Excitation maximum λ_{exc}^{max}. [c] EtOH/MeOH (4/1). [d] Acetonitrile. [e] Value could not be determined.

Even in the absorption spectra alone, a significant influence of the solvent can be seen. Figure 15 shows absorption spectra of $[(\mathbf{1a})Ru(tpy)]^{2+}$ and $[(\mathbf{1a})Ru(tpy)]^{3+}$ in water/acetonitrile (4/1) and EtOH/MeOH (4/1). It can be seen that the band of

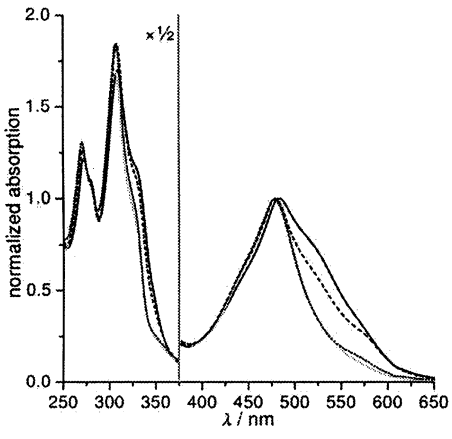

Figure 15. Absorption spectra of $[(\mathbf{1a})Ru(tpy)]^{2+}$ in water/acetonitrile (4/1) (grey) and EtOH/MeOH (4/1) (solid) and of $[(\mathbf{1a})Ru(tpy)]^{3+}$ in water/acetonitrile (4/1) (dotted) and EtOH/MeOH (4/1) (dashed).

$[(\mathbf{1a})Ru(tpy)]^{2+}$ assigned to the ferrocenyl-based MLCT transition (cf. Figure 7 and the discussion in the section on

UV/Vis Spectroscopy above) coincides with the major absorption peak at about 480 nm for this species in water/acetonitrile, whereas it manifests as a shoulder at about 525 nm in the case of EtOH/MeOH. The shoulder is present at the same location in pure acetonitrile (not shown in Figure 15). It cannot be observed for $[(\mathbf{1c})\mathrm{Ru(tpy)}]^{2+}$ and $[(\mathbf{1e})\mathrm{Ru(tpy)}]^{2+}$.

For a more detailed determination of luminescence properties, we have used the novel excitation-emission spectroscopy approach described by Brockhinke et al.[32] As a representative case, the excitation-emission spectrum (EES) of $[(\mathbf{1a})\mathrm{Ru(tpy)}]^{2+}$ is shown in Figure 16. Here, the y axis

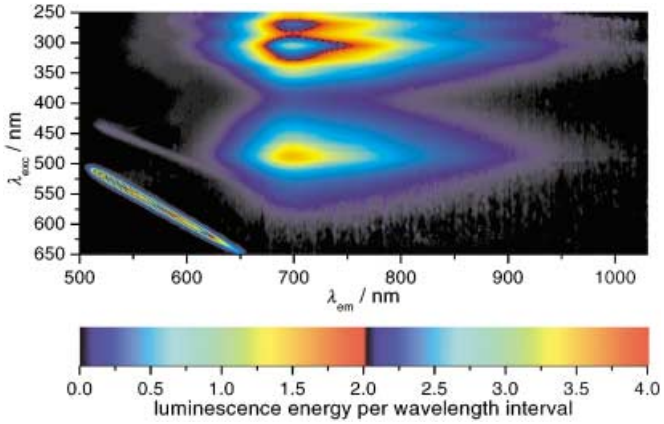

Figure 16. Three-dimensional excitation-emission spectrum (EES) of $[(\mathbf{1a})\mathrm{Ru(tpy)}]^{2+}$ at room temperature in water/acetonitrile (4/1). The strongly tilted line visible in the lower left part of the image is due to Rayleigh scattering, and the accompanying weaker red-shifted line is due to Raman scattering of the solvent.

corresponds to the excitation and the x axis to the emission wavelength. Intensities are represented by different colours. An EES file contains the complete set of excitation and emission spectra of a given substance. Post-processing allows luminescence spectra at different excitation wavelengths (corresponding to horizontal profiles in the EES) to be recovered, and excitation spectra at different emission wavelengths with an arbitrary bandpass to be determined (corresponding to vertical profiles averaged over a given region). These images are the basis for determining the quantum yields and other spectroscopic information summarised in Table 8.

The emission spectra (i.e., horizontal sections through Figure 16) have the same spectral shape regardless of the excitation wavelength and differ only in intensity. The emission spectrum of $[(\mathbf{1a})\mathrm{Ru(tpy)}]^{2+}$ at $\lambda_{exc}^{max} = 489$ nm is plotted in Figure 17. It consists of a single, asymmetric band spanning the region $650 \leq \lambda \leq 850$ nm with a maximum at $\lambda_{max} = 699$ nm. This shows that a single excited state is responsible for all emission observed. In addition, Figure 17 shows a comparison between the absorption spectrum and the excitation spectrum at λ_{exc}^{max}. To allow identification of absorption bands leading to radiationless decay, the spectra are scaled with the constriction that no crossovers are allowed (i.e., the excitation spectrum must always be lower in intensity than the absorption spectrum). The bands at $\lambda = 273$ nm and $\lambda = 309$ nm are much more pronounced in absorption than in emission. This is not unexpected, since generally many states (including nonluminescent ones) are accessible by internal conversion after initial excitation of a highly energetic state. Additionally, two shoulders appear in the absorption, but not in the excitation spectra (at $\lambda = 450$ nm and $\lambda = 525$ nm). The

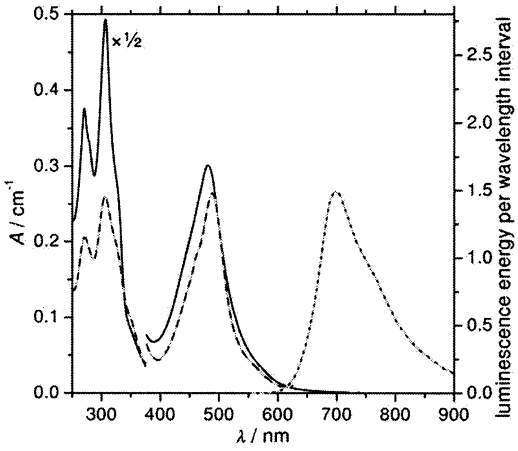

Figure 17. Absorption spectrum (solid), excitation spectrum at $\lambda_{em} = 700$ nm (dashed) and emission spectrum at $\lambda_{exc} = 489$ nm (dotted) of $[(\mathbf{1a})\mathrm{Ru(tpy)}]^{2+}$ at room temperature in water/acetonitrile (4/1).

low-energy shoulder at 525 nm has already been assigned to a ferrocenyl-based MLCT transition (vide supra). It is likely that the shoulder at 450 nm is also due to the ferrocenyl moiety, since relevant ferrocene derivatives absorb in this spectral region (cf. Tables 1 and 4) and are known to be nonluminescent.[3]

Closer inspection of the region between 400 and 600 nm reveals that these bands are quite pronounced for complexes of **1a** in all solvents investigated (Figure 18). The maximum of the excitation spectrum is always red-shifted and does not exhibit the band at 525 nm. In contrast, excitation and absorption maxima are nearly congruent for complexes containing **1c** and **1e**, which have longer spacers than **1a**.

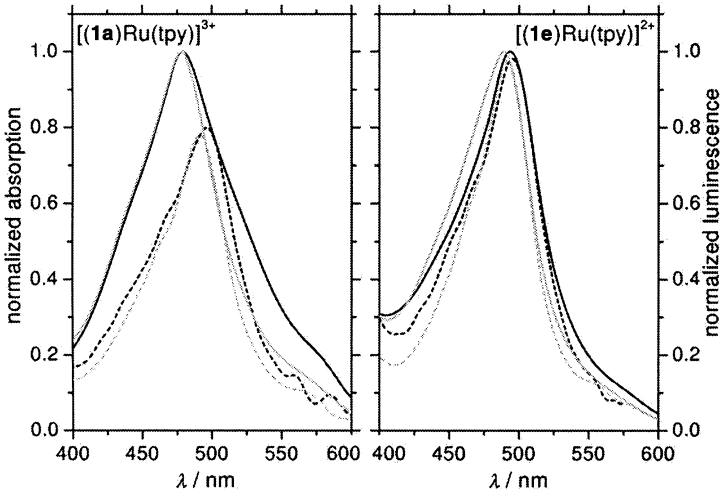

Figure 18. Comparison of absorption (solid) and excitation spectra (dashed) in acetonitrile (black) and water/acetonitrile (4/1) (grey) for $[(\mathbf{1a})\mathrm{Ru(tpy)}]^{3+}$ and $[(\mathbf{1e})\mathrm{Ru(tpy)}]^{2+}$. The other compounds investigated did not show sufficient luminescence in acetonitrile.

The room-temperature luminescence quantum yields (Table 8) are very small for the compounds investigated and are strongly dependent on the solvent. Additionally, as can be derived from Figure 16, they also crucially depend on the excitation wavelength and, whenever possible, were therefore determined at λ_{exc}^{max}, the maximum of the excitation spectrum. As a sideline, we note that the quantum yields depend strongly on the concentration of oxygen in the solvent, as is typical for triplet states.[33]

There is not an exact correlation between these data and the excited-state lifetimes determined by laser flash photolysis under essentially identical conditions of solvent and temperature (Table 5). However, the general trend comes out very well, differentiating clearly between complexes of **1c** (short lifetimes, low quantum yields) on the one hand, and **1a** and **1e** (long lifetimes, high quantum yields) on the other. As a caveat we note that the strong solvent and temperature dependence of the luminescence data emphasises that a comparative interpretation of data obtained under different experimental conditions is fraught with problems. For example, the homoleptic $[(\mathbf{1a})_2Ru]^{2+}$ is not luminescent at 77 K in EtOH/MeOH (4/1). At room temperature in water/acetonitrile (4/1) it exhibits the strongest emission of all compounds investigated, whereas in EtOH/MeOH (4/1) its luminescence is negligible. Interestingly, the strong solvent dependence of quantum yield and spectroscopic structure is not observed for the non-ferrocenylated compounds $[Ru(bpy)_3]^{2+}$ and $[Ru(tpy)_2]^{2+}$. Here, absorption and excitation spectra are nearly congruent and do not change with the solvent. Quantum yields vary by less than 30% for EtOH/MeOH (4/1), water/acetonitrile (4/1) and acetonitrile, $\Phi_{average}$ being 0.05 for $[Ru(bpy)_3]^{2+}$ and 10^{-5} for $[Ru(tpy)_2]^{2+}$. This finding indicates that the strong solvatochromism observed for the other complexes is due to the ferrocenyl moiety.

Conclusion

We have undertaken a systematic study of redox-functionalised bis(terpyridine)ruthenium(II) complexes, which constitute donor–sensitiser dyads or triads of well-defined architecture. We were able to vary independently molecular parameters relevant to electron and energy transfer, namely, the redox potential of the donor unit and the rigid π spacer between the donor and the sensitiser. The ground-state HOMO and LUMO energies were probed by electrochemical methods. The redox-active units rigidly connected in the di- and trinuclear species investigated are essentially independent of one another. Excited-state properties were probed by absorption, transient absorption and luminescence spectroscopy. Complexes functionalised with the electron-rich Fc# groups have very short lived excited states that show no room-temperature luminescence and are only weakly emissive, even at 77 K in frozen glassy solution. Complexes containing the less electron-rich ferrocenyl groups are emissive in fluid solution at room temperature, particularly when an acetylenic substituent is directly attached to the terpyridine ligand, which leads to excited state lifetimes of up to 0.3 μs. This behaviour is unprecedented for this class of compounds. Oxidation of the donor group blocks the pathway of reductive quenching and leads to more strongly luminescent species.

Following the arguments already outlined by Hutchison et al. for Ru^{II} complexes of Fc-tpy′,[6] we propose an energy level diagram (Figure 19) for our Ru^{II} complexes.

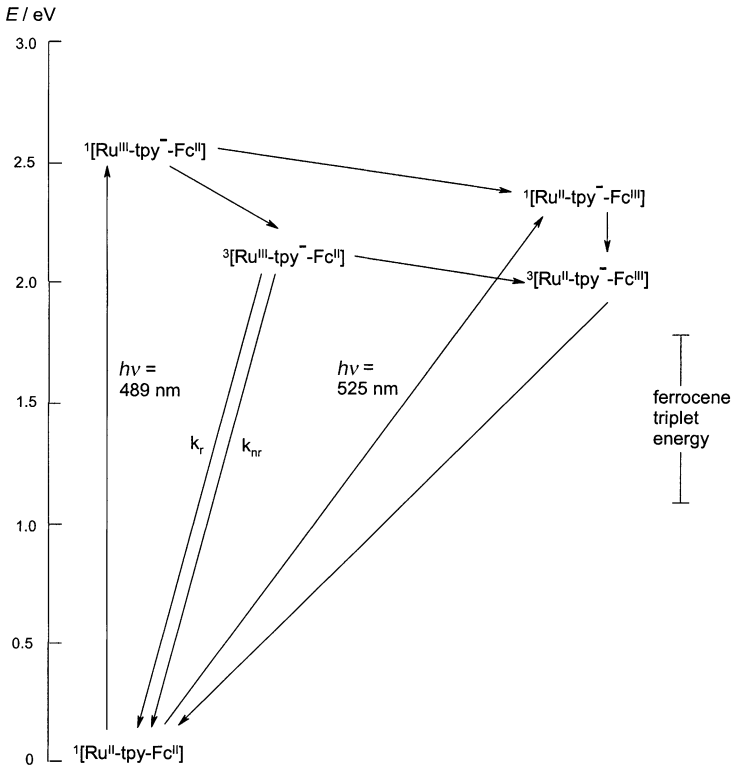

Figure 19. Energy level diagram for $[(\mathbf{1a})Ru(tpy)]^{2+}$ and related complexes.

For $[(\mathbf{1a})Ru(tpy)]^{2+}$, the absorption maximum at 489 nm, which is attributable to the ruthenium-based transition $^1[(d(\pi)^6)] \rightarrow {}^1[(d(\pi)^5)(\pi^*_{tpy})^1]$, places the excited state denoted $^1[Ru^{III}\text{-}tpy^-\text{-}Fc^{II}]$ at an energy of about 2.5 eV. The transition $^1[(d(\pi)^6_{Fc})] \rightarrow {}^1[(d(\pi)^5_{Fc})(\pi^{*Ru}_{tpy})^1]$ leading to the shoulder at 525 nm corresponds to an energy of about 2.4 eV for the excited state denoted $^1[Ru^{II}\text{-}tpy^-\text{-}Fc^{III}]$. The energy of the corresponding nonemissive triplet state denoted $^3[Ru^{II}\text{-}tpy^-\text{-}Fc^{III}]$ can be estimated from the low-energy onset of the underlying absorption band (ca. 610 nm, Figure 7), giving a value of about 2.0 eV. The energy of the luminescent triplet state $^3[Ru^{III}\text{-}tpy^-\text{-}Fc^{II}]$ at 77 K may be approximated to be about 2.1 eV from the emission maximum (600 nm, Figure 14). At room temperature the emission profile is structureless with a maximum at about 700 nm, and no meaningful interpretation in terms of excited-state energies is possible.

Similar energy level schemes may be obtained, mutatis mutandis, for the other complexes investigated. For the Fc#-substituted compounds, the energy of the ferrocenyl-based states shown on the right-hand side of Figure 19 is lowered by about 0.1 eV. In any case, the energies of the excited triplet states shown in Figure 19 most likely lie above the triplet energy of ferrocene, which has been estimated to be between 1.1[34] and 1.8 eV,[35] and the ferrocenyl-centred triplet state of

our compounds is expected to be located somewhere in this region as the lowest-lying excited state.

Originally, we had hoped to shed more light on the intramolecular quenching mechanisms operative in the present systems, addressing particularly the competition between reductive quenching and quenching by energy transfer. However, it remains unclear whether the results obtained previously in this vein for intermolecular quenching of photoexcited $[Ru(bpy)_3]^{2+}$ (bpy = 2,2′-bipyridine) by ferrocenes of different redox potentials are transferable to our system.[30] The main reason is that the excited-state lifetimes, although remarkably long for the class of compounds investigated, are still too short for a meaningful interpretation of experiments with chemical quenchers. This clearly is a drawback of Ru^{II} terpyridine complexes in general, and we are therefore currently investigating related systems based on ferrocenyl-functionalised 1,10-phenanthroline ligands, which should lead to much longer lived excited states.[36]

Experimental Section

General: Compounds **1c**, **1d**, [(**1c**)$RuCl_2$(dmso)], [(**1d**)$RuCl_2$(dmso)], [(**1c**)$_2$Ru]$(PF_6)_2$, [(**1d**)$_2$Ru]$(PF_6)_2$ and [(**1c**)Ru(tpy)]$[PF_6]_2$ were described previously by us.[5] Compounds **2a**,[8] **2b**,[11] **3a**,[9] **3b**,[10] **4**,[12] **6a**,[13] $[RuCl_2(dmso)_4]$,[18] [(tpy)$RuCl_3$][19] and acetylferrocenium tetrafluoroborate[37] were prepared according to, or by slight modification of, published procedures. All other compounds are commercially available. Soluble ruthenium(III) chloride hydrate with a ruthenium content of about 38 % was used. Synthetic work involving air-sensitive compounds was performed under an atmosphere of dry argon or nitrogen by using standard Schlenk techniques or a conventional glove box. Solvents and reagents were appropriately dried and purified. Methods and instrumentation used for electrochemistry,[38] EPR spectroscopy,[39] transient absorption spectroscopy[40]and low-temperature luminescence spectroscopy[41] have been previously described. Excitation-emission spectra were obtained by utilising a custom-built setup with a 75 W Xe lamp, two astigmatism-corrected spectrometers for signal processing and a back-thinned CCD camera (Roper Scientific) for detection. Details of this method can be found elsewhere.[32] Samples for electrochemical and photophysical experiments were freshly prepared and handled under nitrogen, since otherwise degradation was observed. A flow cell was used for transient absorption spectroscopy to rule out the accumulation of degradation products. NMR: Bruker Avance DRX 500 and Varian Unity INOVA 500 (500.13 MHz for ^{1}H); MS: VG Autospec (EI; LSIMS, 3-nitrobenzyl alcohol matrix) or Esquire 3000 (ESI); UV/Vis: Perkin Elmer Lambda 9; elemental analyses: Beller (Göttingen), H. Kolbe (Mülheim an der Ruhr) and microanalytical laboratory of the University of Bielefeld.

1a: A solution of ethynylferrocene (**3a**; 680 mg, 3.24 mmol), 4′-(trifluoromethylsulfonyloxy)-2,2′:6′,2″-terpyridine (**2a**; 1.24 g, 3.24 mmol) and $[Pd(PPh_3)_4]$ (230 mg, 0.20 mmol) in toluene (20 mL) and diisopropylamine (10 mL) was stirred at 60 °C for 14 h. The mixture was allowed to cool to room temperature. Volatile components were removed in vacuo. The residue was taken up with dichloromethane (50 mL). Methanol (5 mL) was added and the mixture filtered through a pad of Florisil. The filtrate was reduced to dryness in vacuo. The residue was suspended in methanol (10 mL). The orange solid was isolated by filtration and dried in vacuo. Yield 1.00 g (70 %). ^{1}H NMR ($CDCl_3$): δ = 4.25 (s, 5H), 4.28 (s, 2H), 4.53 (s, 2H), 7.32 – 7.34 (m, 2H), 7.83 – 7.87 (m, 2H), 8.50 (s, 2H), 8.60 (“d”, apparent J = 7.9 Hz, 2H), 8.70 ppm (“d”, apparent J = 4.4 Hz, 2H); ^{13}C{^{1}H} NMR ($CDCl_3$): δ = 63.9, 69.4, 70.1, 71.8, 84.2, 94.0, 121.2, 122.5, 123.9, 134.1, 136.9, 149.1, 155.4, 155.8 ppm; MS (ESI): m/z: 464 [**1a**+Na]$^+$; elemental analysis (%) calcd for $C_{27}H_{19}N_3Fe$ (441.3): C 73.48, H 4.33, N 9.52; found: C 73.27, H 4.75, N 9.27.

1b: By a procedure analogous to that described for **1a**, 2.01 g (62 %) of **1b** was obtained as a red solid from ethynyloctamethylferrocene (**3b**; 1.07 g, 3.23 mmol), 4′-(trifluoromethylsulfonyloxy)-2,2′:6′,2″-terpyridine (**2a**; 1.23 g, 3.23 mmol) and $[Pd(PPh_3)_4]$ (230 mg, 0.20 mmol) in toluene (20 mL) and diisopropylamine (10 mL). ^{1}H NMR ($CDCl_3$): δ = 1.69 (s, 6H), 1.74 (s, 6H), 1.80 (s, 6H), 1.96 (s, 6H), 3.34 (s, 1H), 7.33 – 7.35 (m, 2H), 7.84 – 7.87 (m, 2H), 8.47 (s, 2H), 8.61 (“d”, apparent J = 8.0 Hz, 2H), 8.72 ppm (“d”, apparent J = 4.1 Hz, 2H); ^{13}C{^{1}H} NMR ($CDCl_3$): δ = 9.0, 10.0, 10.7, 10.8, 63.9, 71.7, 81.0, 81.3, 81.8, 82.8, 88.3, 94.9, 121.4, 122.1, 123.9, 135.0, 136.9, 149.1, 155.4, 156.1 ppm; MS (ESI): m/z: 553 [**1b**]$^+$; elemental analysis (%) calcd for $C_{35}H_{35}N_3Fe$ (553.5): C 75.94, H 6.37, N 7.59; found: C 75.60, H 6.68, N 7.01.

1e: $[PdCl_2(PPh_3)_2]$ (5.1 mg, 7 μmol) and CuI (0.5 mg, 3 μmol) were added to a solution of **6a** (120 mg, 0.39 mmol) and 4′-(trifluoromethylsulfonyloxy)-2,2′:6′,2″-terpyridine (**2a**; 148 mg, 0.39 mmol) in diethylamine (5 mL). The mixture was stirred for 16 h. The orange solid was isolated by filtration and dried in vacuo. Yield 144 mg (68 %). ^{1}H NMR ($CDCl_3$): δ = 4.24 (s, 7H), 4.50 (s, 2H), 7.33 – 7.35 (m, 2H), 7.46 – 7.51 (m, 4H), 7.84 – 7.88 (m, 2H), 8,56 (s, 2H), 8.60 (“d”, apparent J = 7.8 Hz, 2H), 8.70 ppm (“d”, apparent J = 4.4 Hz, 2H); ^{13}C{^{1}H} NMR ($CDCl_3$): δ = 64.8, 69.0, 70.0, 71.5, 85.5, 89.0, 91.1, 93.6, 121.2, 121.4, 122.8, 124.0, 124.7, 131.4, 131.8, 133.3, 136.9, 149.2, 155.6, 155.6 ppm; MS (ESI): m/z: 564 [**1e**+Na]$^+$; elemental analysis (%) calcd for $C_{35}H_{23}N_3Fe$ (541.4): C 77.64, H 4.28, N 7.76; found: C 76.90, H 4.73, N 6.77.

1f: $[PdCl_2(PPh_3)_2]$ (10.0 mg, 14 μmol) and CuI (1.0 mg, 5 μmol) were added to **6b** (320 mg, 0.76 mmol) and 4′-(trifluoromethylsulfonyloxy)-2,2′:6′,2″-terpyridine (**2a**; 290 mg, 0.76 mmol) in diethylamine (10 mL). The mixture was stirred for 16 h. Insoluble material was removed by filtration. The filtrate was reduced to dryness in vacuo. The residue was suspended in methanol (5 mL). The orange solid was isolated by filtration and dried in vacuo. Yield 240 mg (48 %). ^{1}H NMR ($CDCl_3$): δ = 1.68 (s, 6H), 1.72 (s, 6H), 1.78 (s, 6H), 1.89 (s, 6H), 3.35 (s, 1H), 7.33 – 7.35 (m, 2H), 7.46 – 7.51 (m, 4H), 7.84 – 7.88 (m, 2H), 8.56 (s, 2H), 8.60 (“d”, apparent J = 7.9 Hz, 2H), 8.71 ppm (“d”, apparent J = 4.4 Hz, 2H); ^{13}C{^{1}H} NMR ($CDCl_3$): δ = 8.7, 9.8, 10.3, 10.9, 64.4, 72.1, 78.2, 81.1, 81.7, 81.9, 84.2, 85.6, 88.9, 93.8, 120.7, 121.2, 122.7, 124.0, 130.8, 131.9, 133.92, 136.9, 149.2, 155.5, 155.7 ppm; MS (ESI): m/z: 653 [**1f**]$^+$; elemental analysis (%) calcd for $C_{43}H_{39}N_3Fe$ (653.7): C 79.01, H 6.01, N 6.43; found: C 78.88, H 6.18, N 6.31.

5b: $[Pd(PPh_3)_4]$ (100 mg, 60 μmol) was added to a solution of ethynyloctamethylferrocene (**3b**; 451 mg, 1.40 mmol) and 4-(bromophenylethynyl)trimethylsilane (**4**; 354 mg, 1.38 mmol) in *n*-propylamine (20 mL). The mixture was stirred at 60 °C for 14 h and subsequently allowed to cool to room temperature. Volatile components were removed in vacuo. The residue was extracted with *n*-hexane (30 mL). Insoluble material was removed by filtration. The filtrate was reduced to dryness in vacuo. The residue was suspended in methanol (10 mL), and the orange solid isolated by filtration. Yield 550 mg (80 %). ^{1}H NMR ($CDCl_3$): δ = 0.23 (s, 9H), 1.68 (s, 6H), 1.74 (s, 6H), 1.78 (s, 6H), 1.89 (s, 6H), 3.32 (s, 1H), 7.38 ppm (s, 4H); ^{13}C{^{1}H} NMR ($CDCl_3$): δ = 0.0, 8.9, 10.0, 10.6, 10.8, 64.4, 71.6, 80.9, 81.1, 81.2, 82.2, 89.0, 91.0, 95.5, 105.0, 121.5, 125.1, 130.8, 131.9 ppm; MS (ESI): m/z: 494 [**5b**]$^+$; elemental analysis (%) calcd for $C_{31}H_{38}FeSi$ (494.6): C 75.28, H 7.74; found: C 74.31, H 7.55.

6b: Potassium fluoride (71 mg, 1.22 mg) was added to a solution of **5b** (550 mg, 1.11 mmol) in a mixture of THF (20 mL) and methanol (10 mL). The mixture was stirred for 16 h. Volatile components were removed in vacuo. The residue was extracted with *n*-hexane (30 mL). The extract was filtered through a pad of Florisil and reduced to dryness in vacuo. Methanol (10 mL) was added to the residue. The orange solid was isolated by filtration and dried in vacuo. Yield 320 mg (68 %). ^{1}H NMR ($CDCl_3$): δ = 1.72 (s, 6H), 1.78 (s, 6H), 1.82 (s, 6H), 1.94 (s, 6H), 3.17 (s, 1H), 3.35 (s, 1H), 7.45 ppm (s, 4H); ^{13}C{^{1}H} NMR ($CDCl_3$): δ = 8.9, 10.0, 10.6, 10.8, 64.3, 71.6, 78.3, 80.7, 81.1, 81.3, 82.2, 83.6, 88.9, 91.1, 120.4, 125.4, 130.9, 132.1 ppm; MS (ESI): m/z: 422 [**6b**]$^+$; elemental analysis (%) calcd for $C_{28}H_{30}Fe$ (422.4): C 79.62, H 7.16; found: C 78.70, H 7.12.

[(1a)$_2$Ru](PF$_6$)$_2$·2H$_2$O: A suspension of **1a** (106 mg, 0.24 mmol) and $[RuCl_2(dmso)_4]$ (58 mg, 0.12 mmol) in ethanol (20 mL) was heated to reflux for 30 min. The solution was allowed to cool to room temperature and filtered through a pad of Celite. A saturated aqueous solution of ammonium hexafluorophosphate (5 mL) was added. The crude product was isolated by filtration and washed with diethyl ether (10 mL). Purification was achieved by column chromatography (Florisil, eluent acetonitrile/water/saturated aqueous potassium nitrate 7/0.5/1). Yield

23.6 mg (15%). ^{1}H NMR (CD_3CN): $\delta = 4.40$ (s, 10H), 4.50 (s, 4H), 4.75 (s, 4H), 7.17–7.19 (m, 4H), 7.40 (d, $J = 5.3$ Hz, 4H), 7.92–7.95 (m, 4H), 8.54 (d, $J = 8.0$ Hz, 4H), 8.81 ppm (s, 4H); ^{13}C{^{1}H} NMR (CD_3CN): $\delta = 71.3$, 73.1, 125.6, 125.9, 128.6, 139.2, 153.6, 156.2, 158.6 ppm; MS (LSIMS): *m/z*: 984 [(**1a**)$_2$Ru]$^+$; elemental analysis (%) calcd for $C_{54}H_{42}N_6F_{12}Fe_2O_2P_2Ru$ (1309.7): C 49.52, H 3.23, N 6.42; found: C 48.60, H 3.16, N 6.00.

[(1e)$_2$Ru](PF$_6$)$_2$·2H$_2$O: *N*-Ethylmorpholine (0.2 mL) was added to a suspension of **1e** (100 mg, 19 μmol) and $RuCl_3 \cdot n H_2O$ (26.7 mg, 9.3 μmol) in ethanol (20 mL). The mixture was heated to reflux for 3 h. The solution was allowed to cool to room temperature and filtered through a pad of Celite. A saturated aqueous solution of ammonium hexafluorophosphate (5 mL) was added. The product was isolated by filtration and washed with diethyl ether (10 mL). Yield 40.0 mg (14%). ^{1}H NMR ([D$_6$]DMSO): $\delta =$ 4.31 (s, 10H), 4.40 (s, 4H), 4.62 (s, 4H), 7.27–7.20 (m, 4H), 7.57 (d, $J =$ 5.6 Hz, 4H), 7.68 ("d", apparent $J = 8.1$ Hz, 4H), 7.75 ("d", apparent $J =$ 8.1 Hz, 4H), 8.04–8.07 (m, 4H), 8.91 (d, $J = 8.1$ Hz, 4H), 9.34 ppm (s, 4H); ^{13}C{^{1}H} NMR ([D$_6$]DMSO): $\delta = 69.4$, 69.9, 71.3, 85.0, 88.8, 92.3. 94.0, 120.1, 124.8, 125.6, 127.9, 129.1, 131.7, 132.1, 138.3, 152.4, 154.8, 157.3 ppm; MS (ESI): *m/z*: 592 [(**1e**)$_2$Ru]$^{2+}$; elemental analysis (%) calcd for $C_{70}H_{50}N_6F_{12}Fe_2O_2P_2Ru$ (1509.9): C 55.68, H 3.33, N 5.56; found: C 56.19, H 3.63, N 5.39.

[(1f)$_2$Ru](PF$_6$)$_2$·2H$_2$O: By a procedure analogous to that described for [(**1e**)$_2$Ru](PF$_6$)$_2$·2H$_2$O, 20.1 mg (11%) of [(**1f**)$_2$Ru](PF$_6$)$_2$·2H$_2$O was obtained from the reaction of **1f** (70.0 mg, 0.11 mmol) and $RuCl_3 \cdot n H_2O$ (15.4 mg, 5.4 μmol) in ethanol (20 mL) in the presence of *N*-ethylmorpholine (0.2 mL). ^{1}H NMR ([D$_6$]DMSO): $\delta = 1.5$ (br s, 24H), 7.13–7.17 (m, 4H), 7.32 (m, 4H), 7.36 ("d", apparent $J = 5.4$ Hz, 4H), 7.55 (m, 4H), 7.89–7.93 (m, 4H), 8.46 (d, $J = 8.1$ Hz, 4H), 8.81 ppm (s, 4H); MS (ESI): *m/z*: 704 [(**1f**)$_2$Ru]$^{2+}$; elemental analysis (%) calcd for $C_{86}H_{82}N_6F_{12}Fe_2O_2P_2Ru$ (1734.3): C 59.56, H 4.77, N 4.85; found: C 60.02; H, 4.85, N, 5.23.

[(1a)Ru(tpy)](PF$_6$)$_2$·2H$_2$O: *N*-ethylmorpholine (0.2 mL) was added to a suspension of **1a** (92.4 mg, 0.15 mmol) and [(tpy)RuCl$_3$] (64.7 mg, 0.15 mmol) in ethanol (10 mL). The mixture was heated to reflux for 3 h. The solution was allowed to cool to room temperature and filtered through a pad of Celite. A saturated aqueous solution of ammonium hexafluorophosphate (5 mL) was added. The crude product was isolated by filtration and washed with diethyl ether (5 mL). Purification was achieved by column chromatography (basic alumina, eluent acetone/water 19/1). Yield 130 mg (42%). ^{1}H NMR (CD_3CN): $\delta = 4.40$ (s, 5H), 4.50 (s, 2H), 4.74 (s, 2H), 7.15–7.17 (m, 4H), 7.33 (d, $J = 5.5$ Hz, 2H), 7.39 (d, $J = 5.4$ Hz, 2H), 7.89–7.94 (m, 4H), 8.41 (t, $J = 8.1$ Hz, 1H), 8.47–8.50 (m, 4H), 8.76 (d, $J =$ 8.1 Hz, 2H), 8.78 ppm (s, 2H); ^{13}C{^{1}H} NMR (CD_3CN): $\delta = 70.6$, 71.2, 71.3, 73.1, 83.9, 99.2, 124.7, 125.4, 125.5, 125.8, 128.4, 128.6, 131.9, 137.0, 139.1, 153.5, 156.2, 158.6, 158.9 ppm; MS (LSIMS): *m/z*: 776 [(**1a**)Ru(tpy)]$^+$; elemental analysis (%) calcd for $C_{42}H_{34}N_6F_{12}FeO_2P_2Ru$ (1101.6): C 45.79, H 3.11, N 7.63; found: C 45.34, H 3.46, N 7.55.

[(1b)Ru(tpy)](PF$_6$)$_2$·2H$_2$O: Triethylamine (0.2 mL) was added to a suspension of **1b** (60.1 mg, 0.11 mmol) and [(tpy)RuCl$_3$] (45.5 mg, 0.10 mmol) in ethanol/water (2/1) (15 mL). The mixture was heated to reflux for 1 h. The solution was allowed to cool to room temperature and filtered through a pad of Celite. A saturated aqueous solution of ammonium hexafluorophosphate (5 mL) was added. The product was isolated by filtration and washed with diethyl ether (5 mL). Yield 42 mg (34%). ^{1}H NMR (CD_3CN): $\delta = 1.5$ (br s, 24H), 7.15–7.16 (m, 4H), 7.32 (d, $J = 4.7$ Hz, 2H), 7.40 (d, $J = 4.7$ Hz, 2H), 7.89–7.92 (m, 4H), 8.41 (t, $J = 8.0$ Hz, 1H), 8.51–8.54 (m, 4H), 8.71 (s, 2H), 8.77 ppm (d, $J = 8.0$ Hz, 2H); ^{13}C{^{1}H} NMR (CD_3CN): $\delta = 124.6$, 125.2, 125.3, 128.3, 128.4, 136.8, 138.8, 139.0, 153.3, 156.1, 156.8, 158.1, 158.8 ppm (Fc$^\#$ C atoms not observed); MS (LSIMS): *m/z*: 888 [(**1b**)Ru(tpy)]$^+$; elemental analysis (%) calcd for $C_{50}H_{50}N_6F_{12}FeO_2P_2Ru$ (1213.8): C 49.48, H 4.15, N 6.92; found: C 49.24, H 4.29, N 6.82.

[(1d)Ru(tpy)](PF$_6$)$_2$·2H$_2$O: *N*-ethylmorpholine (0.2 mL) was added to a suspension of **1d** (92.4 mg, 0.15 mmol) and [(tpy)RuCl$_3$] (64.7 mg, 0.15 mmol) in ethanol (10 mL). The mixture was heated to reflux for 3 h. The solution was allowed to cool to room temperature and filtered through a pad of Celite. A saturated aqueous solution of ammonium hexafluorophosphate (5 mL) was added. The product was isolated by filtration and washed with diethyl ether (5 mL). Yield 91 mg (51%). ^{1}H NMR ([D$_6$]DMSO): $\delta = 1.5$ (br s, 24H), 7.23–7.27 (m, 4H), 7.41 (d, $J = 5.4$ Hz, 2H), 7.52 (d, $J = 5.3$ Hz, 2H), 8.00–8.06 (m, 4H), 8.53 (t, $J = 8.1$ Hz, 1H), 8.83 (d, $J = 8.1$ Hz, 2H), 9.07–9.10 (m, 4H), 9.43 ppm (s, 2H); ^{13}C{^{1}H} NMR (CD_3CN): $\delta = 7.7$, 9.3, 100.7, 124.7, 120.7, 124.0, 124.5, 124.8, 126.7, 127.7, 128.1, 130.1, 134.3, 135.9, 138.0, 138.1, 146.2, 152.1, 152.2, 154.7, 155.1, 157.7, 157.9 ppm (Fc$^\#$ ring C atoms not observed); MS (LSIMS): *m/z*: 964 [(**1d**)Ru(tpy)]$^+$; elemental analysis (%) calcd for $C_{56}H_{54}N_6F_{12}FeO_2P_2Ru$ (1289.9): C 52.14, H 4.22, N 6.52; found: C 52.74, H 4.09, N 6.53.

[(1e)Ru(tpy)](PF$_6$)$_2$·2H$_2$O: By a procedure analogous to that described for [(**1d**)Ru(tpy)](PF$_6$)$_2$·2H$_2$O, 110 mg (64%) of [(**1e**)Ru(tpy)](PF$_6$)$_2$·2H$_2$O was obtained from the reaction of **1e** (81.2 mg, 0.15 mmol) and [(tpy)RuCl$_3$] (66.0 mg, 0.15 mmol) in ethanol (20 mL) in the presence of *N*-ethylmorpholine (0.3 mL). ^{1}H NMR (CD_3CN): $\delta = 4.28$ (s, 5H), 4.36 (s, 2H), 4.56 (s, 2H), 7.14–7.19 (m, 4H), 7.34 (d, $J = 5.4$ Hz, 2H), 7.37 (d, $J =$ 5.3 Hz, 2H), 7.62 ("d", apparent $J = 8.2$ Hz, 2H), 7.75 ("d", apparent $J =$ 8.2 Hz, 2H), 7.89–7.95 (m, 4H), 8.43 (t, $J = 8.1$ Hz, 1H), 8.47–8.50 (m, 4H), 8.74 (d, $J = 8.1$ Hz, 2H), 8.86 ppm (s, 2H); ^{13}C{^{1}H} NMR (CD_3CN): $\delta = 70.4$, 70.9, 72.5, 85.8, 88.7, 93.1, 97.3, 121.4, 124.7, 124.8, 125.4, 125.5, 126.1, 126.2, 128.4, 130.7, 132.6, 133.2, 139.3, 153.4, 156.1, 158.3, 158.5, 158.9 ppm; MS (ESI): *m/z*: 438 [(**1e**)Ru(tpy)]$^{2+}$; elemental analysis (%) calcd for $C_{50}H_{42}N_6F_{12}FeO_2P_2Ru$ (1201.7): C 49.97, H 3.19, N 6.99; found: C 49.23, H 3.56, N 6.72.

[(1c)Ru(1d)](PF$_6$)$_2$·2H$_2$O: A suspension of **1d** (54.0 mg, 0.10 mmol) and [(**1c**)RuCl$_2$(dmso)] (80.0 mg, 0.10 mmol) in ethanol (30 mL) was heated to 80 °C for 2.5 h. The solution was allowed to cool to room temperature and filtered through a pad of Celite. A saturated aqueous solution of ammonium hexafluorophosphate (5 mL) was added. The product was isolated by filtration and washed with diethyl ether (5 mL). Yield 51 mg (38%). ^{1}H NMR ([D$_6$]DMSO): $\delta = 1.5$ (br s, 24H), 4.34 (s, 5H), 4.42 (s, 2H), 4.65 (s, 2H), 7.26 (m, 4H), 7.53 (m, 6H), 7.86 (m, 2H), 8.05 (m, 4H), 8.28 (m, 2H), 8.50 (m, 2H), 9.06 (m, 2H), 9.13 (m, 2H), 9.42 (m, 2H), 9.52 ppm (s, 2H); ^{13}C{^{1}H} NMR (CD_3CN): $\delta = 7.7$, 9.3, 100.7, 124.7, 120.7, 124.0, 124.5, 124.8, 126.7, 127.7, 128.1, 130.1, 134.3, 135.9, 138.0, 138.1, 146.2, 152.1, 152.2, 154.7, 155.1, 157.7, 157.9 ppm (Fc$^\#$ ring C atoms not observed); MS (LSIMS): *m/z*: 1248 [(**1c**)Ru(**1d**)]$^+$; elemental analysis (%) calcd for $C_{74}H_{66}N_6F_{12}Fe_2O_2P_2Ru$ (1574.1): C 56.47, H 4.23, N 5.34; found: C 56.47, H 4.27, N 5.49.

[(1a)Ru(tpy)][BF$_4$](PF$_6$)$_2$·2H$_2$O: A solution of [(**1a**)Ru(tpy)](PF$_6$)$_2$·2H$_2$O (100 mg, 91 μmol) and acetylferrocenium tetrafluoroborate (30.0 mg, 95 μmol) in acetonitrile (10 mL) was stirred for 15 h. Volatile components were removed in vacuo. The residue was dissolved in acetone (10 mL) and filtered through a pad of Celite. The volume of the filtrate was reduced to about 3 mL. The product was precipitated by dropwise addition of diethyl ether, isolated by filtration, washed with diethyl ether (2 × 5 mL) and dried in vacuo. Yield 90 mg (83%). Elemental analysis (%) calcd for $C_{42}H_{34}N_6BF_{16}FeO_2P_2Ru$ (1188.4): C 42.45, H 2.88, N 7.07; found: C 42.37, H 2.97, N 7.25.

[(1d)Ru(tpy)](PF$_6$)$_3$·2H$_2$O: By a procedure analogous to that described for [(**1a**)Ru(tpy)](BF$_4$)(PF$_6$)$_2$·2H$_2$O, 98 mg (83%) of [(**1d**)Ru(tpy)](PF$_6$)$_2$·2H$_2$O was obtained from the reaction of [(**1d**)Ru(tpy)](PF$_6$)$_2$·2H$_2$O (100 mg, 82 μmol) and ferrocenium hexafluorophosphate (27.2 mg, 82 μmol) in acetonitrile (10 mL). Elemental analysis (%) calcd for $C_{56}H_{53}N_6F_{18}FeO_2P_3Ru$ (1436.9): C 47.02, H 3.72, N 5.85; found: C 46.43, H 3.80, N 5.34.

[(1a)$_2$Zn](PF$_6$)$_2$·2H$_2$O: A suspension of **1a** (406 mg, 0.92 mmol) and zinc tetrafluoroborate (110 mg, 0.46 mmol) in ethanol (50 mL) was heated to reflux for 3 h. The solution was allowed to cool to room temperature and filtered through a pad of Celite. A saturated aqueous solution of ammonium hexafluorophosphate (10 mL) was added. The product was isolated by filtration and washed with diethyl ether (10 mL). Yield 390 mg (67%). ^{1}H NMR (CD_3CN): $\delta = 4.41$ (s, 10H), 4.56 (s, 4H), 4.78 (s, 4H), 7.40–7.43 (m, 4H), 7.83 (d, $J = 5.0$ Hz, 4H), 8.15–8.19 (m, 4H), 8.57 (d, $J =$ 8.0 Hz, 4H), 8.75 ppm (s, 4H); ^{13}C{^{1}H} NMR (CD_3CN): $\delta = 71.4$, 71.8, 73.4, 125.6, 124.1, 125.8, 128.6, 142.3 148.4, 149.1, 150.5 ppm; MS (ESI): *m/z*: 473 [(**1a**)$_2$Zn]$^{2+}$; elemental analysis (%) calcd for $C_{54}H_{42}N_6F_{12}Fe_2O_2P_2Zn$ (1274.0): C 50.91, H 3.32, N 6.60; found: C 51.16, H 3.34, N 6.53.

[(1d)$_2$Zn](PF$_6$)$_2$·2H$_2$O: By a procedure analogous to that described for [(**1a**)$_2$Zn](PF$_6$)$_2$·2H$_2$O, 330 mg (75%) of [(**1d**)$_2$Zn](PF$_6$)$_2$·2H$_2$O was obtained from the reaction of **1d** (337 mg, 0.54 mmol) and zinc tetrafluoroborate (64.0 mg, 0.27 mmol) in ethanol (50 mL). ^{1}H NMR (CD_3CN): $\delta =$ 1.7 (br s, 24H), 7.42–7.44 (m, 4H), 7.84–7.86 (m, 8H), 8.18–8.21 (m, 8H), 8.75 (d, $J = 8.2$ Hz, 4H), 9.00 ppm (s, 4H); ^{13}C{^{1}H} NMR (CD_3CN): $\delta = 9.0$, 9.9, 10.6, 10.8, 122.2, 124.2, 128.5, 128.9, 129.4, 132.4, 135.3, 142.2, 148.9, 149.0, 150.8, 156.5 ppm (Fc$^\#$ ring C atoms not observed); MS (ESI): *m/z*:

Table 9. X-ray crystallographic data.

Compound	**1a**	**1b**	**1c**	$[(\mathbf{1a})_2Zn](PF_6)_2\cdot 2CH_3CN$
empirical formula	$C_{27}H_{19}FeN_3$	$C_{35}H_{35}FeN_3$	$C_{33}H_{23}FeN_3$	$C_{58}H_{44}F_{12}Fe_2N_8P_2Zn$
formula weight	441.30	553.51	517.39	1320.02
temperature [K]	173	173	293	100
crystal system	orthorhombic	monoclinic	orthorhombic	monoclinic
space group	*Pbca*	$P2_1/c$	$Pca2_1$	$P2_1/c$
a [Å]	10.929(4)	12.397(4)	10.050(2)	24.9130(2)
b [Å]	12.128(4)	12.718(4)	10.070(2)	12.7280(1)
c [Å]	30.734(6)	18.708(6)	48.860(10)	17.3790(3)
β [°]		92.59(3)		104.1260(6)
V [Å^3]	4074(2)	2946.6(16)	4944.8(17)	5344.12(11)
Z	8	4	8	4
ρ_{calcd} [g cm^{-3}]	1.439	1.248	1.390	1.641
μ [mm^{-1}]	0.760	0.539	0.638	1.132
$F(000)$	1824	1168	2144	2672
crystal size [mm]	$0.6\times0.6\times0.2$	$0.9\times0.7\times0.2$	$0.4\times0.3\times0.1$	$0.2\times0.2\times0.1$
θ range [°]	2.3–30.0	1.9–25.0	2.6–28.0	3.0–27.5
reflections collected	5925	5436	17880	86174
independent reflections	5925	5180	8697	12205
R_{int}		0.0486	0.0797	0.077
reflections with $I>2\sigma(I)$	3809	3467	4687	8189
parameters	356	360	667	750
GOF on F^2	1.021	1.027	0.855	1.027
$R1$[a] ($I>2\sigma(I)$/$wR2$)[b]	0.0537/0.1207	0.0610/0.1470	0.0557/0.1318	0.0490/0.1260
largest diff. peak/hole [e Å^{-3}]	0.477/−0.385	0.303/−0.300	0.422/−0.341	0.537/−0.538

[a] $R1=\Sigma||F_o|-|F_c||/\Sigma|F_o|$. [b] $wR2=\{\Sigma[w(F_o^2-F_c^2)^2]/\Sigma[w(F_o^2)^2]\}^{0.5}$.

673 $[(\mathbf{1d})_2Zn]^{2+}$; elemental analysis (%) calcd for $C_{84}H_{82}N_6F_{12}Fe_2O_4P_2Zn$ (1706.6): C 59.12, H 4.84, N 4.92; found: C 58.94, H 5.25, N 5.47.

$[(\mathbf{1a})_2Fe](PF_6)_2$: A suspension of **1a** (221 mg, 0.50 mmol) and iron(II) chloride (31.8 mg, 0.25 mmol) in ethanol (50 mL) was heated to reflux for 3 h. The solution was allowed to cool to room temperature and filtered through a pad of Celite. A saturated aqueous solution of ammonium hexafluorophosphate (10 mL) was added. The crude product was isolated by filtration, washed with diethyl ether (10 mL) and dissolved in acetone (5 mL). The product was precipitated by dropwise addition of diethyl ether, isolated by filtration and washed with diethyl ether (2×5 mL). Yield 190 mg (62%). ^{1}H NMR (CD_3CN): $\delta=4.44$ (s, 10H), 4.56 (s, 4H), 4.81 (s, 4H), 7.09–7.12 (m, 4H), 7.16 (d, $J=4.9$ Hz, 4H), 7.89–7.92 (m, 4H), 8.48 (d, $J=7.9$ Hz, 4H), 8.93 ppm (s, 4H); ^{13}C{^{1}H} NMR (CD_3CN): $\delta=63.3$, 71.3, 71.5, 73.2, 84.2, 100.5, 124.9, 125.8, 128.5, 134.3, 139.8, 154.1, 158.4, 161.0 ppm; MS (ESI): m/z: 469 $[(\mathbf{1a})_2Fe]^{2+}$; elemental analysis (%) calcd for $C_{54}H_{38}N_6F_{12}Fe_3P_2$ (1228.4): C 52.79, H 3.18, N 6.84; found: C 53.55, H 3.86, N 6.78.

X-ray crystallography: The crystal structure of **1d** has already been published.[5] X-ray crystallographic data for **1a**, **1b**, **1c** and $[(\mathbf{1a})_2Zn](PF_6)_2$ are collected in Table 9. A Siemens $P2_1$ four-circle diffractometer was used for **1a** and **1b**, whereas data collection was performed with a STOE IPDS diffractometer for **1c** and a Nonius Kappa CCD diffractometer for $[(\mathbf{1a})_2Zn](PF_6)_2$. Graphite-monochromatised $Mo_{K\alpha}$ radiation ($\lambda=0.71073$ Å) was used in each case. The structures were solved by direct methods. Programs used were Siemens SHELXTL PLUS[42] and SHELXL 97.[43] Full-matrix least-squares refinement on F^2 was carried out anisotropically for the non-hydrogen atoms. Hydrogen atoms were included at calculated positions by using a riding model. CCDC-192337 (**1a**), CCDC-192338 (**1b**), CCDC-192339 (**1c**) and CCDC-192342 ($[(\mathbf{1a})_2Zn](PF_6)_2$) contain the supplementary crystallographic data for this paper. These data can be obtained free of charge via www.ccdc.cam.ac.uk/conts/retrieving.html (or from the Cambridge Crystallographic Data Centre, 12 Union Road, Cambridge CB2 1EZ, UK; fax: (+44) 1223-336-033; or deposit@ccdc.cam.uk).

Acknowledgement

This work was generously supported by the Deutsche Forschungsgemeinschaft, the Volkswagen Foundation and the Fonds der Chemischen Industrie. We are grateful to Degussa AG for a generous gift of precious-metal compounds. We thank Prof. Franco Scandola and Dr. Rainer Bausch for helpful discussions, and Dr. Olaf Kruse for help with low-temperature emission studies. Prof. Piero Zanello gratefully acknowledges the financial support from the University of Siena (PAR 2001).

[1] Reviews: a) V. Balzani, S. Campagna, G. Denti, A. Juris, S. Serroni, M. Venturi, *Acc. Chem. Res.* **1998**, *31*, 26–34; b) J.-P. Collin, P. Gaviña, V. Heitz, J.-P. Sauvage, *Eur. J. Inorg. Chem.* **1998**, 1–14; c) F. R. Keene, *Coord. Chem. Rev.* **1997**, *166*, 121–159; d) F. Barigelletti, L. Flamigni, J.-P. Collin, J.-P. Sauvage, *Chem. Commun.* **1997**, 333–338; e) A. Harriman, R. Ziessel, *Chem. Commun.* **1996**, 1707–1716; f) V. Balzani, A. Juris, M. Venturi, S. Campangna, S. Serroni, *Chem. Rev.* **1996**, *96*, 759–833; g) J.-P. Sauvage, J.-P. Collin, J.-C. Chambron, S. Guillerez, C. Coudret, V. Balzani, F. Barigelletti, L. De Cola, L. Flamigni, *Chem. Rev.* **1994**, *94*, 993–1019; h) K. Kalyanasundaram, *Photochemistry of Polypyridine and Porphyrin Complexes*, Academic Press, London, **1992**; i) V. Balzani, F. Barigeletti, L. De Cola, *Top. Curr. Chem.* **1990**, *158*, 31–71; j) A. Juris, V. Balzani, F. Barigelletti, S. Campagna, P. Belser, A. von Zelewsky, *Coord. Chem. Rev.* **1988**, *84*, 85–277.

[2] See, for example, a) P. Lainé, F. Bedioui, E. Amouyal, V. Albin, F. Berruyer-Penaud, *Chem. Eur. J.* **2002**, *8*, 3162–3176; b) P. Lainé, F. Bedioui, P. Ochsenbein, V. Marvaud, M. Bonin, E. Amouyal, *J. Am. Chem. Soc.* **2002**, *124*, 1364–1377; c) J.-P. Collin, S. Guillerez, J.-P. Sauvage, F. Barigelletti, L. De Cola, L. Flamigni, V. Balzani, *Inorg. Chem.* **1995**, *34*, 2759–2767.

[3] Review: S. Fery-Forgues, B. Delavaux-Nicot, *J. Photochem. Photobiol. A: Chem.* **2000**, *132*, 137–159.

[4] See, for example, a) P. D. Beer, A. R. Graydon, L. R. Sutton, *Polyhedron* **1996**, *15*, 2457–2461; b) P. D. Beer, F. Szemes, V. Balzani, C. M. Salà, M. G. B. Drew, S. W. Dent, M. Maestri, *J. Am. Chem. Soc.* **1997**, *119*, 11864–11875.

[5] Part of this work has been briefly communicated: U. Siemeling, U. Vorfeld, B. Neumann, H.-G. Stammler, P. Zanello, F. Fabrizi de Biani, *Eur. J. Inorg. Chem.* **1999**, 1–5.

[6] K. Hutchison, J. C. Morris, T. A. Nile, J. L. Walsh, D. W. Thompson, J. D. Petersen, J. R. Schoonover, *Inorg. Chem.* **1999**, *38*, 2516–2523.

[7] K. Sonogashira in *Metal-catalyzed Cross-coupling Reactions* (Eds.: F. Diederich, P. J. Stang), Wiley-VCH, Weinheim, **1998**, Chap. 5.
[8] K. T. Potts, D. Konwar, *J. Org. Chem.* **1991**, *56*, 4815–4816.
[9] J. Polin, H. Schottenberger, B. Anderson, S. F. Martin, *Org. Synth.* **1996**, *73*, 262–266.
[10] P. Jutzi, B. Kleinebekel, *J. Organomet. Chem.* **1997**, *545–546*, 573–576.
[11] P. Korall, A. Börje, P.-O. Norrby, B. Åkermark, *Acta Chem. Scand.* **1997**, *51*, 760–766.
[12] M. G. Steinmetz, C. Yu, L. Li, *J. Am. Chem. Soc.* **1994**, *116*, 932–943.
[13] R. P. Hsung, C. E. D. Chidsey, L. R. Sita, *Organometallics* **1995**, *14*, 4808–4815.
[14] A. G. Orpen, *Chem. Soc. Rev.* **1993**, *22*, 191–197.
[15] P. Seiler, J. Dunitz, *Acta Crystallogr. Sect. B* **1979**, *35*, 1068–1074.
[16] D. P. Freyberg, J. L. Robbins, K. N. Raymond, J. C. Smart, *J. Am. Chem. Soc.* **1979**, *101*, 892–897.
[17] See, for example: a) J.-C. Chambron, C. Coudret, J.-P. Sauvage, *New. J. Chem.* **1992**, *16*, 361–363; b) E. C. Constable, A. M. W. Cargill Thompson, *J. Chem. Soc. Dalton Trans.* **1992**, 3467–3475.
[18] I. P. Evans, A. Spencer, G. Wilkinson, *J. Chem. Soc. Dalton Trans.* **1973**, 204–209.
[19] C. A. Bessel, R. A. Leising, L. F. Szczepura, W. J. Perez, M. H. V. Huyhn, K. J. Takeuchi, K. J. Brewer, S. W. Jones *Inorg. Synth.* **1998**, *32*, 186–198.
[20] a) C. Stroh, P. Turek, P. Rabu, R. Ziessel, *Inorg. Chem.* **2001**, *40*, 5334–5342; b) N. W. Alcock, P. R. Barker, J. M. Haider, M. J. Hannon, C. L. Painting, Z. Pikramenou, E. A. Plummer, K. Rissanen, P. Saarenketo, *J. Chem. Soc. Dalton Trans.* **2000**, 1447–1461; c) B. Whittle, E. L. Horwood, L. H. Rees, S. R. Batten, J. C. Jeffery, M. D. Ward, *Polyhedron* **1998**, *17*, 373–379.
[21] J. P. Lozos, B. M. Hoffman, C. G. Franz, *QCPE* **1973**, *11*, 243.
[22] a) Y. S. Sohn, D. N. Hendrickson, H. B. Gray, *J. Am. Chem. Soc.* **1971**, *93*, 3603–3612; b) M. M. Rohmer, A. Veillard, M. H. Wood, *Chem. Phys. Lett.* **1974**, *29*, 466–468; c) D. R. Cott, R. S. Becker, *J. Chem. Phys.* **1961**, *35*, 516–531.
[23] J. R. Winkler, T. L. Netzel, C. Creutz, N. Sutin, *J. Am. Chem. Soc.* **1987**, *109*, 2381–2392.
[24] F. Scandola, personal communication.
[25] a) A. C. Benniston, V. Grosshenny, A. Harriman, R. Ziessel, *Angew. Chem.* **1994**, *106*, 1956–1958; *Angew. Chem. Int. Ed. Engl.* **1994**, *33*, 1884–1885; b) M. Hissler, A. El-ghayoury, A. Harriman, R. Ziessel, *Angew. Chem.* **1998**, *110*, 1804–1807; *Angew. Chem. Int. Ed.* **1998**, *37*, 1717–1720.
[26] B. Farlow, T. A. Nile, J. L. Walsh, A. T. McPhail, *Polyhedron* **1993**, *12*, 2891–2894.
[27] J. N. Demas, G. A. Crosby, *J. Am. Chem. Soc.* **1971**, *93*, 2841–2847.
[28] M. L. Stone, G. A. Crosby, *Chem. Phys. Lett.* **1981**, *79*, 169–173.
[29] P. Zanello in *Ferrocenes* (Eds.: A. Togni, T. Hayashi), VCH, Weinheim, **1995**, Chap. 7.
[30] E. J. Lee, M. S. Wrighton, *J. Am. Chem. Soc.* **1991**, *113*, 8562–8564.
[31] J. N. Demas, G. A. Crosby, *J. Phys. Chem.* **1971**, *75*, 991–1024.
[32] A. Brockhinke, R. Plessow, P. Dittrich, K. Kohse-Höinghaus, *Appl. Phys. B* **2000**, *71*, 755–763.
[33] J. R. Lakowicz, *Principles of Fluorescence Spectroscopy*, 2nd ed., Plenum, New York, **1999**.
[34] V. Balzani, F. Bolletta, L. Moggi, *Spectrosc. Lett.* **1978**, *11*, 525–535.
[35] A. Maciejewski, A. Jaworska-Augustiniak, Z. Szeluga, J. Woytrzak, J. Karolczak, *Chem. Phys. Lett.* **1988**, *153*, 227–232.
[36] U. Siemeling, K. Bausch, poster presented at the 5th Symposium of the Volkswagen Foundation on Intra- and Inter-molecular Electron Transfer, Chemnitz, **2001**.
[37] N. G. Conelly, W. E. Geiger, *Chem. Rev.* **1996**, *96*, 877–910.
[38] A. Togni, M. Hobi, G. Rihs, G. Rist, A. Albinati, P. Zanello, D. Zech, H. Keller, *Organometallics* **1994**, *13*, 1224–1234.
[39] C. Bianchini, F. Laschi, D. Masi, F. M. Ottaviani, A. Pastor, M. Peruzzini, P. Zanello, F. Zanobini, *J. Am. Chem. Soc.* **1993**, *115*, 2723–2730.
[40] a) J. Hockhertz, S. Steenken, K. Wieghardt, P. Hildebrandt, *J. Am. Chem. Soc.* **1993**, *115*, 11222–11230; b) S. Steenken, R. A. McClelland, *J. Am. Chem. Soc.* **1990**, *112*, 9648–9649; c) G. Gurzadyan, H. Görner, *Chem. Phys. Lett.* **2000**, *319*, 164–172.
[41] O. Kruse, P. J. Nixon, G. H. Schmid, C. W. Mullineaux, *Photosynth. Res.* **1999**, *61*, 43–51.
[42] G. M. Sheldrick, SHELXTL PLUS, Siemens Analytical Instruments, Madison, WI (USA), **1990**.
[43] G. M. Sheldrick, SHELXL 97, University of Göttingen, Göttingen (Germany), **1997**.

Received: September 11, 2002
Revised: February 24, 2003 [F4412]

